Icarus 226 (2013) 742–759

Contents lists available at SciVerse ScienceDirect

Icarus

journal homepage: www.elsevier.com/locate/icarus

Morphology of fluvial networks on Titan: Evidence for structural control ☆

Devon M. Burr [a,*], Sarah A. Drummond [b], Richard Cartwright [a], Benjamin A. Black [c], J. Taylor Perron [c]

[a] Earth and Planetary Sciences Department, University of Tennessee Knoxville, 1412 Circle Drive, Knoxville, TN 37996-1410, USA
[b] Natural and Behavioral Sciences, Pellissippi State Community College, 10915 Hardin Valley Road, Knoxville, TN 37933-0990, USA
[c] Department of Earth, Atmospheric and Planetary Sciences, Massachusetts Institute of Technology, 77 Massachusetts Ave., Cambridge, MA 02139, USA

ARTICLE INFO

Article history:
Received 1 March 2013
Revised 9 June 2013
Accepted 11 June 2013
Available online 9 July 2013

Keywords:
Saturn, Satellites
Geological processes
Tectonics
Titan, hydrology
Titan, surface

ABSTRACT

Although Titan's surface shows clear evidence of erosional modification, such as fluvial incision, evidence for tectonism has been less apparent. On Earth, fluvial networks with strongly preferred orientations are often associated with structural features, such as faults or joints, that influence flow or erodibility. We delineated and classified the morphologies of fluvial drainages on Titan and discovered evidence of structural control. Fluvial networks were delineated both on synthetic aperture radar (SAR) images covering ~40% of Titan from the Cassini Titan Radar Mapper up through T71 and on visible light images of the Huygens landing site collected by the Descent Imager/Spectral Radiometer (DISR). The delineated networks were assigned to one of three morphologic classes—dendritic, parallel or rectangular—using a quantitative terrestrial drainage pattern classification algorithm modified for use with Titan data. We validated our modified algorithm by applying it to synthetic fluvial networks produced by a landscape evolution model with no structural control of drainage orientations, and confirmed that only a small fraction of the networks are falsely identified as structurally controlled. As a second validation, we confirmed that our modified algorithm correctly classifies terrestrial networks that are classified in multiple previous works as rectangular. Application of this modified algorithm to our Titan networks results in a classification of rectangular for one-half of the SAR and DISR networks. A review of the geological context of the four terrestrial rectangular networks indicates that tensional stresses formed the structures controlling those terrestrial drainages. Based on the similar brittle response of rock and cryogenic ice to stress, we infer that structures formed under tension are the most likely cause of the rectangular Titan networks delineated here. The distribution of these rectangular networks suggests that tensional stresses on Titan may have been widespread.

1. Introduction

Like Earth, Titan has a thick, nitrogen-rich atmosphere that participates in an active volatile cycle and produces a range of processes that modify the surface. Clouds of methane, which constitutes ~5% of Titan's troposphere, have been observed to form and dissipate over various regions of Titan, implying rainfall (e.g., Griffith et al., 2000; Porco et al., 2005; Lunine and Atreya, 2008; Atreya et al., 2009; Turtle et al., 2011). Rain has also been inferred from in situ observations near Titan's equator (Tomasko et al., 2005). As a result of this precipitation and associated surface runoff, fluvial networks, thought to be carved into the water ice bedrock (Collins, 2005; Perron et al., 2006) and/or formed by flow across radar-dark plains, are widely distributed (Fig. 1) (Jaumann et al., 2008, 2009; Lorenz et al., 2008; Baugh, 2008; Burr et al., 2009; LeGall et al., 2010; Cartwright et al., 2011; Black et al., 2012; Langhans et al., 2012). Fluvial incision resulting from sapping by subsurface liquid has been suggested to have operated on small networks with stubby tributaries in the northeast wall of Menrva crater (Baugh, 2008) and at the Huygens landing site (Tomasko et al., 2005), although terrestrial analog work implicates the strong role of overland flow in forming such networks (Lamb et al., 2006, 2008; Burr et al., 2012). In the polar regions, the fluvial networks commonly empty into lakes potentially filled with liquid hydrocarbons and nitrogen (Stofan et al., 2007; Mitri et al., 2007; Hayes et al., 2008). In tropical regions, dark dune fields provide evidence that aeolian processes are also an active resurfacing agent (Barnes et al., 2008; Radebaugh et al., 2008). These atmospheric, fluvial, lacustrine, and aeolian features attest to exogenic modification of Titan's surface. That this activity was recent or is on-going is

* Corresponding author.
E-mail address: dburr1@utk.edu (D.M. Burr).

0019-1035/$ - see front matter © 2013 The Authors. Published by Elsevier Inc. All rights reserved.
http://dx.doi.org/10.1016/j.icarus.2013.06.016

supported by Titan's low crater density (Lorenz et al., 2007; Wall et al., 2009; Wood et al., 2010; Neish and Lorenz, 2012).

In contrast to these obvious effects of atmospheric and surficial processes, evidence for internally driven modification of Titan's surface by tectonism or cryovolcanism is ambiguous. Hypothesized cryovolcanic features such as Ganesa Macula, interpreted as a dome, and Winia Fluctus, interpreted as a flow (Sotin et al., 2005; Lopes et al., 2007; Wall et al., 2009), have been questioned or reinterpreted (Moore and Pappalardo, 2011). A few observations suggest that tectonism may have modified Titan's landscape. Linear mountains and valleys inferred in the Xanadu region have been attributed to regional extension, and nearby lineaments have been interpreted as systems of conjugate faults (Radebaugh et al., 2011), but an impact origin for this structure and its lineaments has also been suggested (Brown et al., 2011). Steep breaks in topography close to the Ontario Lacus shoreline may indicate the presence of fault scarps, suggesting that the lake is contained within a graben or rift valley (Wall et al., 2010), but in the low-resolution and noisy Cassini images the geomorphologic identification of these putative tectonic features is inconclusive. Radar bright regions interpreted as eroded mountain chains (Radebaugh et al., 2007) represent no more than ~10% of Titan's surface based on mapping through T30 (Lopes et al., 2010), and the source and sign of the tectonic stresses that would have built such features are unclear. These limited observations to date of possible tectonic structures suggest that either Titan does not have active tectonic processes, or that erosion and deposition by rivers and wind effectively mask and erase their effects (Collins et al., 2010), preventing a critical analysis. A comparison of Titan fluvial network shapes with landscape evolution models suggests either recent resurfacing or slow fluvial incision rates on Titan (Black et al., 2012).

Although fluvial erosion can obscure evidence of tectonically generated landforms, it can also reveal tectonic patterns. Tectonic deformation can generate strongly oriented topographic features that divert surface flows, and fault zones, joints or exposed layering that are more easily erodible. These mechanisms can produce fluvial drainage networks with links oriented in a small number of preferred directions, instead of branching networks in which the orientations of individual links are controlled primarily by the slope direction. An example of the influence of tectonic contraction on drainage may be seen in the Zagros Simply Folded Belt in Iran, where an inferred dendritic pre-fold drainage system was reformed after Mio-Pliocene deformation into a trellis pattern, with the dominant stream azimuths parallel to the NW–SE-trending folds (Burberry et al., 2008). Similarly, in the Nepal Himalaya, large transverse rivers flow longitudinally in alternating directions along mountain fronts north of the Main Boundary thrust, forming a 'gridiron' pattern (Gupta, 1997). In the Argentera Massif (French-Italian Alps), the Pliocene–Pleistocene tectonics have also produced transverse (largely trellis) drainages in some regions, although other regions show dendritic drainages (Ribolini and Spagnolo, 2007). In other collisional settings, such preexisting tectonic influence may be erased by subsequent tectonic modification; for example, a study of correlations between kink-banks and jointing with drainage patterns in the Chamba Nappe of the Himalaya, indicates that the river valleys correspond with orientations with neotectonic joints but not with Precambrian to Upper Paleozoic kink-band structures (Sharma et al., 2003). The influence of tensional tectonic stresses may be seen in southwestern Ontario, where Pleistocene glacial deposits are underlain by Paleozoic bedrock on top of Proterozoic basement. The episodic arching of the basement fractured the strata bedrock into regional joint sets whose orientations correspond both to the buried channels within the bedrock and to the superjacent post-glacial river valleys (Eyles et al., 1997). Complex tectonic histories involving both extension and compression may be inferred with input from drainage analysis; a morphotectonic study of the lower Sangro River valley, central Italy showed that uplift and tilting formed a parallel drainage network during the Middle Pleistocene, after which activity along faults and fractures reorganized drainage into a rectangular network (D'Alessandro et al., 2008).

Our plan view analysis of fluvial drainage networks on Titan indicates biases in substrate erodibility or pre-existing topography, suggesting the influence of tectonic structures on overland flow. For this analysis, we used an empirical terrestrial drainage classification algorithm that has been modified for use with the limited information available from the Cassini–Huygens mission at Titan. This classification algorithm differs from the qualitative classification methods used in previous Titan work in that it makes use of measurable parameters, and it yields somewhat different results as presented here. To validate our modifications to the original classification algorithm and to test the robustness of our results, we applied our modified classification algorithm to both previously classified terrestrial drainages and to fluvial networks generated by a numerical landscape evolution model. For the most common drainage patterns in our Titan data, we explored and discuss the types of stress responsible for such drainage patterns on Earth and the implications for Titan.

2. Background

2.1. Fluvial drainage networks in Cassini–Huygens data

Inferred fluvial features have been detected by three imaging instruments onboard the Cassini spacecraft: the Visual and Infrared Mapping Spectrometer (VIMS), operating at 300–5100 nm (Brown et al., 2004), the Imaging Science Subsystem (ISS), operating over 200–1100 nm (Porco et al., 2005), and the Cassini Titan Radar Mapper (RADAR), emitting at 2.17 cm (Elachi et al., 2005). The datasets for these instruments have a range of spatial resolutions. VIMS and ISS images have surface resolutions that vary with position and emission angle, but are commonly a few kilometers per pixel. The synthetic aperture radar (SAR) data from the RADAR are collected in swaths with the highest resolution (~350 m/pixel) at swath center, corresponding to closest approach, and lower resolution (down to 1.7 km/pixel) at the swath ends. These data constitute the highest resolution dataset available from the Cassini spacecraft. Although they cover less than one-half of the surface to date, compared to near-global coverage by the VIMS and ISS data, the SAR data provide the best resolution for mapping the fluvial networks and sufficient coverage to infer global distributions by network type (Fig. 1). Radar swaths are referred to by their Titan flyby number, T#.

The fluvial networks observed in SAR data can be hundreds of kilometers in length and tens to hundreds of kilometers in width and display a variety of forms (Fig. 2; see also Burr et al., 2012). Initial studies classified the networks on the basis of width and length as well as visual characteristics such as SAR albedo and bright-dark pairing (Lorenz et al., 2008). More recent efforts to map and characterize fluvial networks also used a visual classification scheme (Langhans et al., 2012).

Multiple fluvial networks are also observed in visible light (0.66–1.00 μm) images taken by the Huygens Descent Imager/Spectral Radiometer (DISR) during its descent to the surface of Titan (Tomasko et al., 2005; Soderblom et al., 2007a). The spatial resolutions of DISR images range from 20 to 90 m/pixel for images taken during descent. The networks detected in DISR data (~5–10 km in length, ~100 m in width for individual links; Fig. 3) are significantly smaller than those detected in SAR data and are not discernible in the available overlapping SAR data (Soderblom et al., 2007b).

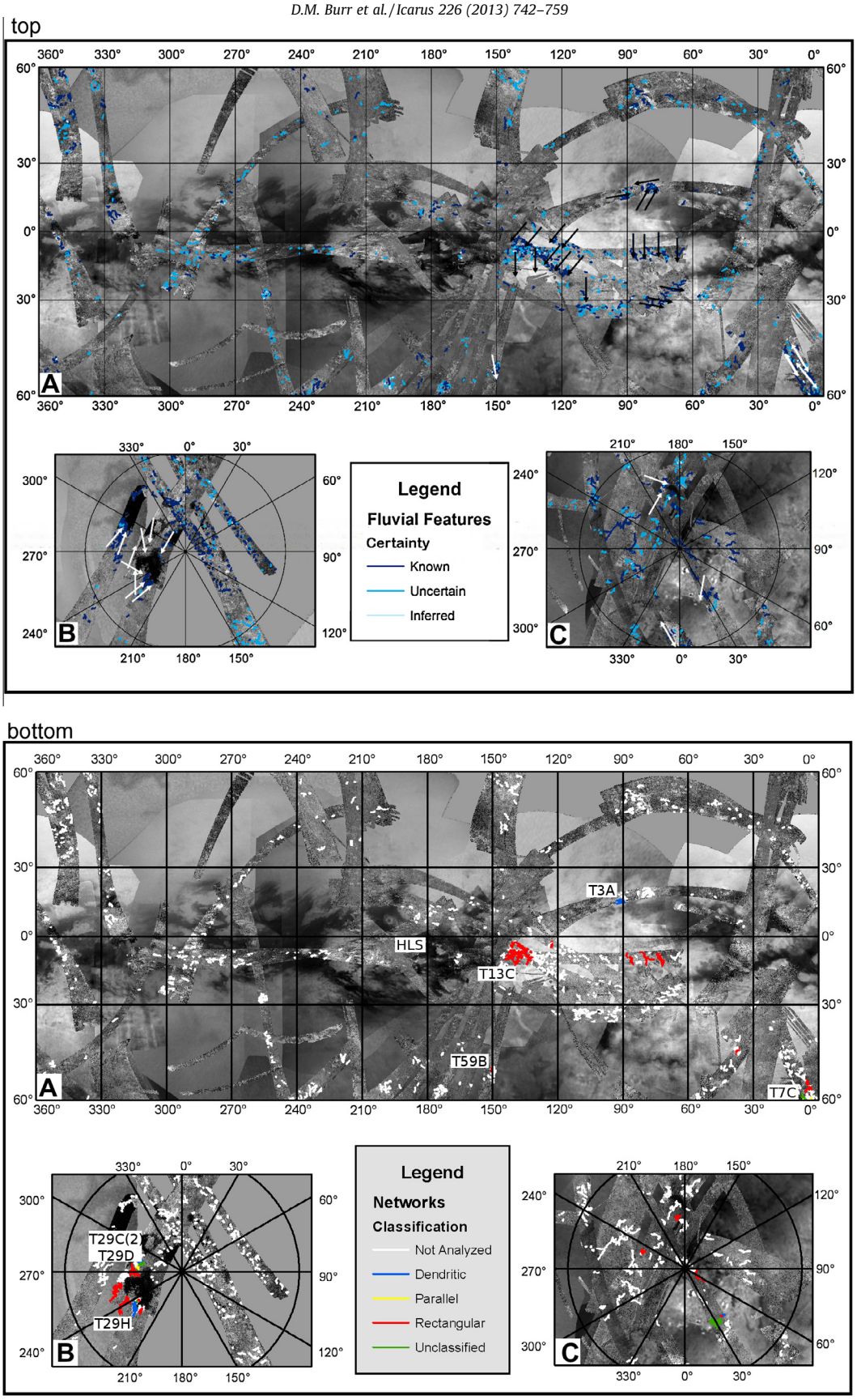

Fig. 1. (top) Geographic distribution of fluvial features as delineated on SAR data up through T71, color-coded according to certainty (see legend). Inferred flow directions are show by both black and white arrows (for best contrast with background). (bottom) Fluvial networks color-coded by network classification (see legend). The white labeled boxes point (with upper or lower left hand corner) to the approximate locations of the example networks shown in Fig. 2, and the Huygens landing site ("HLS") shows the approximate location of the DISR networks showing in Fig. 3. For both top and bottom figures, (B) and (C) show the north and south polar regions, respectively, poleward of ~60° latitude. 10° of longitude is equal to 450 km. Electronic versions (ArcGIS files) of these network delineations in Fig. 1 (bottom) are available at http://web.eps.utk.edu/faculty/burr.html and at http://bit.ly/BurrTitanFluvial. (For interpretation of the references to color in this figure legend, the reader is referred to the web version of this article.)

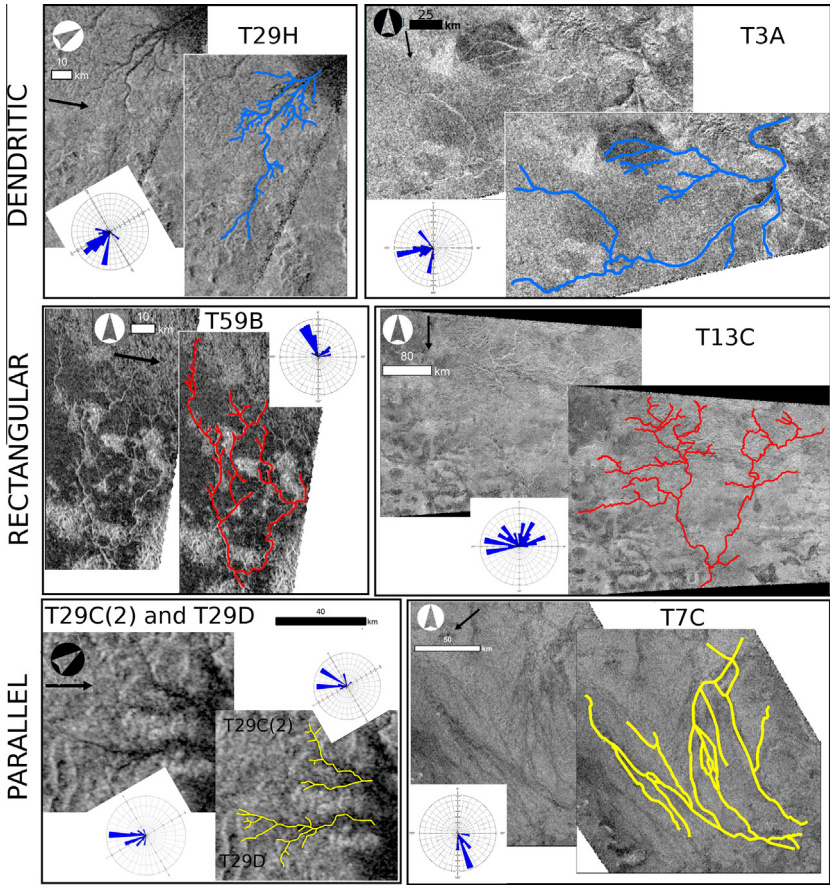

Fig. 2. Examples presented in both raw and delineated images of drainage patterns observed in SAR data; color-coding for delineations follows the same scheme as used in Fig. 1. Rose diagrams show the cumulative length of the links by azimuth in 10° bins (*y*-axes are variable) and are rotated so that north coincides with the north direction (chevrons) on the raw images. Black arrows indicate radar illumination directions. Locations of networks are indicated in Fig. 1 and Table 4. (For interpretation of the references to color in this figure legend, the reader is referred to the web version of this article.)

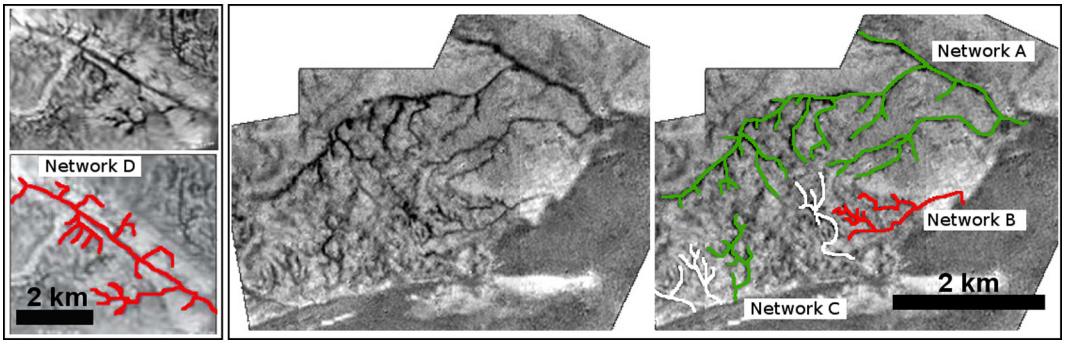

Fig. 3. Raw and delineated images of four networks along Huygens Landing Site "coastline" observed in DISR data. Networks A and C are unclassified; networks B and D are rectangular. Rose diagrams are not included because the lack of projection information renders absolute azimuthal information unreliable. (For interpretation of the references to color in this figure legend, the reader is referred to the web version of this article.)

Even within the limited area shown in the DISR mosaic of the Huygens landing site, the form of the fluvial networks varies. To the east (Network A in Fig. 3), the drainage network has longer and higher-order tributaries and more sinuous links, whereas to the west (Network E), the drainage network shows shorter, stubbier, lower-order tributaries (Tomasko et al., 2005; Soderblom et al., 2007a). This contrast in appearance was interpreted as resulting from differences in fluvial processes and controls (Soderblom et al., 2007a).

While the SAR and DISR data represent a significant engineering achievement and offer a wealth of information, their resolution and noise level place some limits on our view of Titan's drainage networks. The smallest observed tributaries likely do not represent the full extent of most networks (Burr et al., 2012). Thus, while we report values below for the total lengths of the individual links (fluvial features between two junctions) and the Shreve magnitudes of the networks (the number of first-order links), these values are best understood as total *apparent* link lengths and *apparent* Shreve magnitudes. Because of our inability to resolve small fluvial features, the proportions of different network morphologies (Section 3.3) are necessarily based on only the largest known networks, which are a minority of all known networks (Fig. 1, bottom). Lastly,

the character of the links comprising the drainage networks – whether river channels formed directly by flowing liquid, or river valleys which contain a smaller river channel – cannot be determined (see Burr et al., 2012 for discussion). The effects of these uncertainties on our approach and results are discussed at relevant locations in the text below.

2.2. Drainage network types and classification

As on Titan, fluvial networks on Earth exhibit a range of morphologies and sizes. Analysis of network morphology, or drainage pattern, can provide information about regional slope, underlying structures, and bedrock characteristics (Zernitz, 1932; Thornbury, 1954; Howard, 1967; Morisawa, 1985; Twidale, 2004). Combinations of these geologic controls lead to the formation of identifiable drainage network patterns. Because Howard (1967) summarized previous work and is widely relied upon as a definitive source for network classification (e.g., Ritter et al., 2002), we use Howard's terminology, which is also employed in more recent work (e.g., Mejía and Niemann, 2008) (but see Drummond (2012) for a discussion of the slight differences among classification systems).

Basic drainage patterns, such as dendritic, parallel, trellis, and rectangular (Fig. 4), have specific geologic implications (Table 1); modified patterns, which differ from the basic patterns in some regional aspect (e.g., a closer or wider spacing of tributaries), are possible where multiple controls influence drainage (Howard, 1967). From analysis of 198 terrestrial networks qualitatively classified by drainage pattern in the literature, Ichoku and Chorowicz (1994) developed an empirical algorithm that identifies the network attributes and their optimum values that are diagnostic of the four basic drainage patterns in Fig. 4 and in Table 1 – dendritic, parallel, rectangular, and trellis – as well as the pinnate form. Networks not meeting any of the specifications for these five patterns are considered "unclassified." This quantitative algorithm provides measureable criteria derived from a substantial dataset for identification of each drainage pattern, and thereby minimizes reliance on the experience or pattern recognition skills of the investigator. In this algorithm, the optimum values of tributary junction angles, link lengths, link orientations, link curvedness, link meander, and proportion of right angular bends are used to classify networks. These attributes can be measured in the field or from maps or remotely sensed images of sufficiently high resolution.

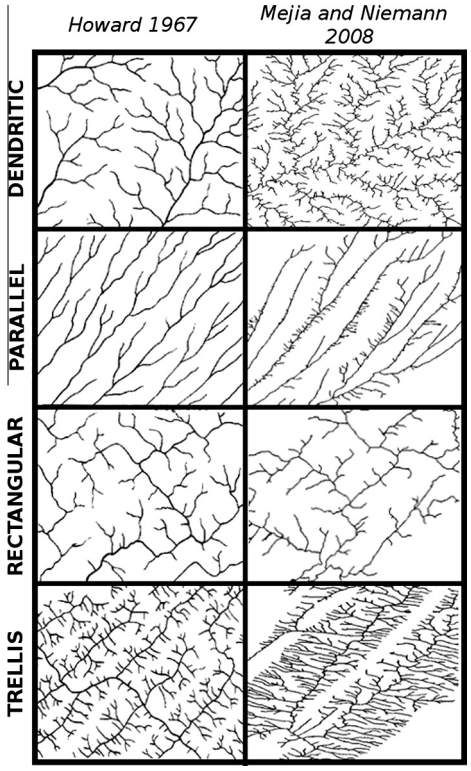

Fig. 4. Four of the basic drainage patterns reproduced from Howard (1967) and from Mejía and Niemann (2008). Flow in all cases is to the lower left. Our drainage pattern algorithm modified from Ichoku and Chorowicz (1994) can detect the upper three patterns – dendritic, parallel, and rectangular. The fourth pattern, trellis, may also have rectangularity but is characterized by shorter external links, which are not detectable in the Titan data due to resolution limits.

Some of the drainage network characteristics used by this algorithm, such as junction angles and interior link lengths, are discernible in the Titan SAR and DISR images. Because of the resolution and quality of the Titan images, however, not all of the attributes required by the original algorithm can be measured. For example, the original algorithm requires measures of channel curvedness and meander, whereas the individual flow channels cannot be reliably discerned in either the DISR or SAR images (Perron et al., 2006; Burr et al., 2012). Similarly, because the termini of external links cannot be reliably determined, external link lengths, required to distinguish between the two rectilinear patterns of rectangular and trellis, cannot be accurately measured. Thus, we cannot use the full algorithm as published (Ichoku and Chorowicz, 1994).

Three network classes, however, are identified only by length and angular characteristics that can be discerned and reliably measured in remotely sensed images of Titan. Thus, we may simplify the algorithm to identify those three classes – dendritic, parallel, and rectangular – as was previously done for a more limited dataset of Titan networks (Burr et al., 2009). The limitations of the classification scheme when applied to low-resolution data and our approach to the resultant potential misclassification are discussed further in Section 5.3.

3. Methods and data

3.1. Titan network delineation

Drainage networks were delineated and classified in both SAR and DISR data. For the SAR data, we used a global map of all SAR swaths through the T71 fly-by on July 7, 2010, prior to a year-long hiatus in SAR data collection (Fig. 1). These data cover ~40% of Titan. Because these data are of variable resolution and often noisy, visual identification of networks may be ambiguous, and the relatively uncommon use of SAR data for terrestrial network analysis adds uncertainty. To systematize network delineation, we followed a set of three criteria derived from previous work (Barnes et al., 2007; Lorenz et al., 2008; Burr et al., 2009): (a) distinguishability in tone (bright or dark) from the surrounding terrain, (b) a bright/dark pairing consistent with illumination direction that is indicative of a trough, and (c) fluviatile morphology, i.e., having sinuous links and/or a branching pattern. The network delineation was accomplished by three mappers (SAD, RC, and BAB) who initially mapped independently on overlapping areas in order to calibrate their feature identification. The results were later checked (DMB and RC) for consistency, both internally and with previous publications. Features meeting two or more of the criteria were characterized as "known;" features meeting one criterion were characterized as "uncertain;" and where features were discontinuous over distances less than ~10 km, the discontinuous sections were characterized as "inferred" (Fig. 5). Links of all levels of certainty (Fig. 1, top) were included in drainage pattern analysis. Previous work with overlapping images has shown that although different radar illumination azimuths may result in some differences (of order a few tens of percent) in network delineation, the network classifications derived

Table 1
Basic drainage patterns (shown in Fig. 4) discussed in this work, with geologic implications from Howard (1967). Dendritic, parallel and rectangular patterns can be detected with the modified drainage pattern classification algorithm used here (Fig. 6). The trellis pattern can be detected using the modified algorithm, but not with the resolution of the Titan data currently available. Additional basic and modified drainage patterns not listed in this table are discussed in the references.

Drainage pattern	Geologic implications
Dendritic	Uniformly resistant rocks and gentle or no consistent regional slope at time of drainage inception
Parallel	Moderate to steep regional slopes and/or parallel, elongate landforms
Rectangular	Joints and/or faults at near-right angles
Trellis	Dipping or folded sedimentary, volcanic, or low-grade metasedimentary rocks with contrasting resistance to erosion

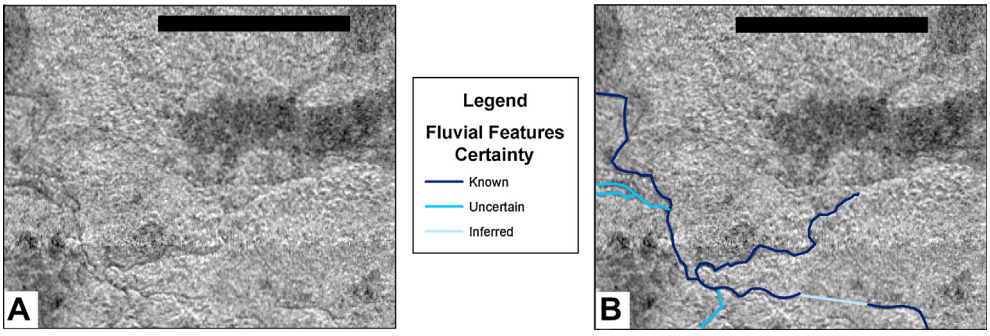

Fig. 5. Example of three categories used to describe link certainty in SAR data. (A) raw SAR image, and (B) SAR image with network tracing. Center of images is approximately 10°S, 87°W in T13 radar swath. Scale bars on both images are 50 km. The horizontal (east–west) band ~1/4 of the way from the image bottom is an artifact produced by overlapping antenna beams.

Table 2
Projections used per latitude range to take measurements for input to the modified classification algorithm.

Latitude range	Projection	Parameter measured
60°–90°N and S	Polar stereographic	Length, angle
60°N–60°S	Equidistant cylindrical	Length
60°N–60°S	Mercator	Angle

from these differently illuminated swaths are the same (Burr et al., 2009) (see Section 3.3 below for discussion of network pattern classification). After mapping was complete, separate equidistant projections (for measuring length) and equal angle projections (for measuring angles) were made for each swath as appropriate for the swath latitude (Table 2). These measurements were collected using the Jennessent Graphic Tools and Shapes plug-in for ArcMap (http://www.jennessent.com/arcgis/shapes_graphics.htm). We also determined the apparent Shreve magnitude and the apparent total link length for each network.

For the drainage networks observed in the DISR data (Fig. 3), we used the DISR mosaic from an altitude of approximately eight kilometers from Tomasko et al. (2005). The fluvial features were delineated in ArcMap based on distinguishability in tone and fluviatile morphology, but because these data were taken under the diffuse lighting conditions at Titan's surface, the third criterion (bright/dark pairing indicative of shadowing) does not apply and certainty classifications were not used. However, comparison with the DISR network delineation in Perron et al. (2006) was used to promote consistency. Length and angle data were collected from this mosaic. Because the mosaic does not contain the information necessary for correct geospatial projection, our measurements may have small errors and absolute link azimuths are unavailable. However, because the area covered is small, any error introduced is considered minimal, consistent with previous use of this mosaic (Tomasko et al., 2005; Perron et al., 2006; Soderblom et al., 2007a).

3.2. Titan network classification

Network drainage patterns were classified using our modified algorithm. A flowchart of this algorithm (Fig. 6) shows both the diagnostic parameters that determine drainage network classification and also the limitations of this technique when applied to low-resolution data. The necessary input parameters for the algorithm are lengths and azimuths of network links, junction angles of first order tributaries, percent of acute (<80°) junction angles in the network, and percents for interior and exterior links of right angle (80–100°) bends, identified as changes in orientation between two straight reaches of at least 5 pixels on each side of the bend (Ichoku and Chorowicz, 1994). Because we cannot discern true exterior links in the Titan data, we used the apparent first order links as the exterior links. After network attributes are measured and necessary percentages computed, networks with a mean exterior link length shorter than 10 pixels are excluded from the analysis, and networks with a mean exterior link length equal to or longer than 10 pixels are tested for rectangularity, parallelism, and dendritic morphology (right side of the algorithm in Fig. 6). Rectangularity may be inferred from one of three conditions: (1) $\geqslant$20% of all links have right angular bends, (2) $\geqslant$50% of order 2 or higher-order links have right angular bends, or (3) for 30° bins of the links comprising the trunk channel, any two orthogonal bins have the two highest length totals by at least 10%. As dictated by the authors of the original algorithm, these tests were applied in this order in which they are listed here. The necessity in the second test for tracking both link magnitude and stream order made manual application of this test difficult for the larger networks, and it was rarely used in our analysis. This omission may artificially reduce the proportion of rectangular networks we detect below the true proportion; our percentage classification of networks as rectangular is therefore considered conservative. If a network passes *any* of these three tests, it is classified as rectangular. If not, it is tested for parallelism. Parallelism may be inferred from one of three conditions: (1) $\geqslant$60% of total exterior link length fall within a single 30° bin, (2) the sum of any two adjacent 30° bins is $\geqslant$70%

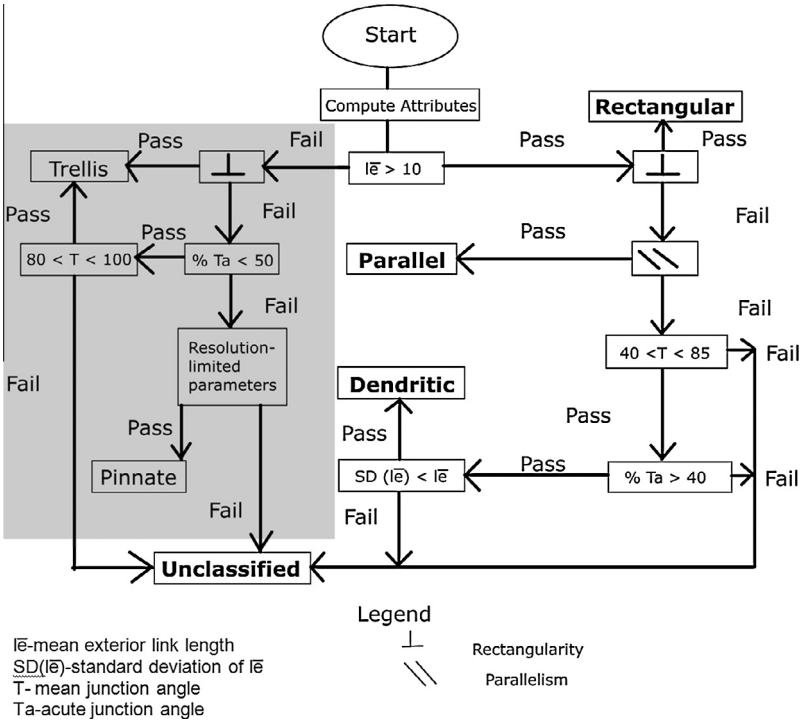

Fig. 6. Drainage pattern classification algorithm based on Ichoku and Chorowicz (1994) modified for use with Titan data. "Resolution-limited parameters" includes channel curvedness and meander. The algorithm as used with current Titan is blind to the classifications on the left, covered by the gray box (see text for discussion).

of total exterior link length, or (3) the total exterior link length in any two adjacent 30° bins is $\geqslant$50% and the total interior link length in the same two bins is $\geqslant$80%. If the network passes *any one* of these three tests, it is classified as parallel. If not, it continues to the three tests for a dendritic network: (1) the mean junction angle is between 40° and 85°, (2) $\geqslant$40% of junction angles are acute, and (3) the standard deviation of mean exterior link length is less than the mean exterior link length. As stipulated in the original algorithm (Ichoku and Chorowicz, 1994), a network must pass *all three* dendritic tests to be classified as dendritic.

These quantitative tests are based on characteristics that were found to be common to networks of a given qualitative classification (Ichoku and Chorowicz, 1994). However, a given characteristic may be common to more than one network morphology; for example, rectangularity is common to both trellis and rectangular networks (Fig. 6). Conversely, a single network could have characteristics of more than one classification. For example, networks may have right angle bends in over half of the order 2 links, thus passing one rectangular test, and also have a moderate mean junction angle with 40% of the junction angles being acute and similar exterior link lengths, thereby passing all three dendritic tests. Thus, in this algorithm, distinguishing among classifications relies on the prescribed order of the tests (Ichoku and Chorowicz, 1994). Rectangular and parallel networks form under particular geologic controls of drainage orientations, whereas dendritic morphologies form in the relative absence of such control. The characteristics of rectangular and parallel networks – right angle bends, link orientations, and link lengths – are therefore assessed first. If the network fails to meet one of those tests, the characteristics for dendritic morphology – junction angle and consistent exterior link lengths – are assessed. The necessity for passing all three dendritic tests does not necessarily imply that it is less likely for a network to be classified as dendritic, but that characteristics of other networks are more distinguishing, whereas characteristics of dendritic networks may also be true of non-dendritic drainage.

With this modified algorithm, networks that do not fall into any of these three classes are unclassified. Under the original algorithm, networks with mean exterior link lengths less than 10 pixels are tested for trellis and pinnate drainages (left side of the algorithm in Fig. 6), which we cannot detect due to the resolution limits of the data. See Ichoku and Chorowicz (1994) for more information on the network classification algorithm.

3.3. Sensitivity analysis of classification to network size

For small networks, the algorithm may produce invalid results where a small number of measurements yields unrepresentative percentages. A quantitative minimum size cutoff is not provided in the original work (Ichoku and Chorowicz, 1994), although sixth order is suggested elsewhere to be a minimum network size for that algorithm, though an explanation for the minimum size is not articulated (Mejía and Niemann, 2008). Many networks imaged in SAR data as well as some DISR networks, had only a few links per network, raising the possibility of misclassification for those smallest networks.

To assess this possibility, we conducted a sensitivity analysis for our data. In our approach, we considered the classifications – and therefore the classification percentages – for the largest networks to be reliable, and assessed whether the classification percentages for the smallest networks were statistically significantly different. From our global network delineations, we chose networks for analysis with a minimum of 10 links, for which the lowest possible Shreve magnitude is 6. For a given network, Horton–Strahler stream order (a measure of stream hierarchy) is always equal to or larger than the Shreve magnitude (the number of upstream links). So a minimum Shreve magnitude of 6 ensures that the suggestion of Mejía and Niemann (2008) is met. Flow directions could not be determined for 3 out of the 48 SAR networks of greater than 10 links, which prevented us from deriving Shreve magnitudes, although it was still possible to classify these networks based on measurements of bend and junction angles. Thus, our sensitivity analysis population consisted of 45 networks with at least 10 links, for which the percentages in each network class were calculated.

Table 3
Number of networks within a given range of apparent Shreve magnitudes. For three of the 48 networks with ambiguous flow directions, Shreve magnitudes could not be derived.

Apparent Shreve magnitudes	Number of networks
6–8	15
9–13	13
14–51	17

To assess the difference between the classification percentages for the largest and the smallest networks, we divided this population of 45 networks into three roughly equal groups by apparent Shreve magnitude (Table 3). We then compared the distribution by network classification for the smallest network group (Shreve magnitudes 6–8, $N = 15$) to those of the largest network group (Shreve magnitudes 14–51, $N = 17$). This comparison was accomplished using a root mean square (RMS) difference in the classification percentages between those two groups, computed as

$$\text{RMS difference} = \sqrt{((x_1 - y_1)^2 + (x_2 - y_2)^2 + (x_3 - y_3)^2 + (x_4 - y_4)^2)/4}$$

where x and y represent the percentages for the smaller and larger networks, and 1, 2, 3, and 4 represent the four classifications (dendritic, parallel, rectangular, and unclassified). The RMS difference for our dataset is 10.10%.

We then determined the probability that this 10.10% RMS difference between the classification percentages for the smallest and largest networks arose by chance. This determination was made using a Monte Carlo simulation of one million iterations. In each iteration, we selected 17 networks at random, computed the classification percentages, and calculated the RMS difference between the randomly selected group and the group of large networks. The resulting distribution of one million RMS difference values (Fig. 7 top) shows that there is a >90% chance of obtaining an RMS value that equals or exceeds 10.10% purely by chance (Fig. 7, bottom). This result implies that there is not a significant difference between the classifications of small and large networks. Based on this calculation, we use all networks with at least 10 links (giving Shreve magnitudes of at least 6 as recommended by Mejía and Niemann (2008)), in our analysis. Total percentages reported below for each network class are for all 48 networks with Shreve magnitudes between 6 and 51.

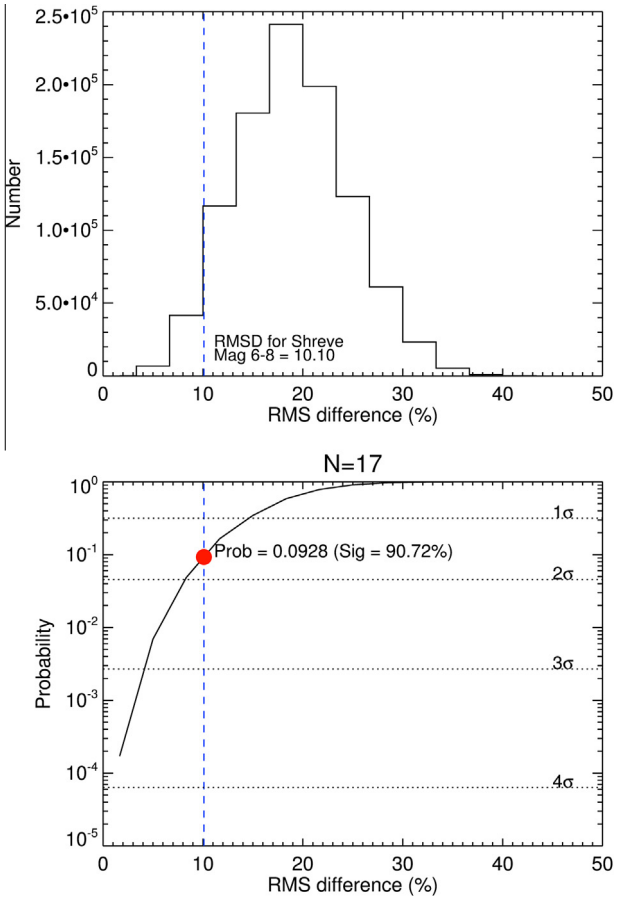

Fig. 7. Plots showing the results of our network size sensitivity analysis. The blue lines on both plots show the actual RMS difference value (11.15%) between the largest and smallest networks for our dataset. (top) The distribution of RMS difference values between the classification percentages of our networks with Shreve magnitudes 14–51 and a Monte Carlo simulation of classification percentages drawn from 44 networks at random. (bottom) A plot of the probability of obtaining any value for the RMS difference between the classification percentages of our networks and the Monte Carlo results. The red dot marks the actual RMS difference between the smallest and largest Titan networks, showing that the likelihood of deriving this RMS difference by random sampling is 8.72%. (For interpretation of the references to color in this figure legend, the reader is referred to the web version of this article.)

3.4. Validation of the modified algorithm using synthetic networks

Application of the modified classification algorithm to our delineated Titan networks resulted in a majority of Titan networks being classified as rectangular (Table 4; see Section 4.2 below). In light of the large percentage of rectangular networks, their geologic implications (Table 1), and the difference from results of previous studies, we considered whether this preponderance of rectangular networks might be the result of a bias introduced by our modification of the terrestrial algorithm. To test for such a bias, we applied our modified algorithm to synthetic drainage networks formed under conditions that should *not* result in rectangular networks and determined what fraction of these networks are classified as rectangular.

The synthetic networks were created with a landscape evolution model (Black et al., 2012) in which the rate of bedrock river incision is proportional to stream power (the rate of energy expenditure by a river's flow) and mass wasting into the channel is parameterized by a slope threshold for the valley side walls. Three separate model landscapes (e.g., Fig. 8) were produced by eroding a mechanically homogeneous substrate with a moderately sloping, randomly rough initial surface. Each model was run for several million model years, and the resultant landscapes hosted 63 networks of at least 10 links, the same minimum size criterion used for analysis of the Titan networks.

When our modified classification algorithm was applied to these 63 networks, three networks passed one of the three tests for rectangular classification and thus were classified as rectangular. This result may be interpreted in one of two ways. One possibility is that none of the synthetic networks are truly rectangular, and our modified algorithm performs incorrectly in a small percentage of cases, falsely classifying ~5% of the networks as rectangular. An alternate interpretation is that, despite a lack of structural control, ~5% of the synthetic networks happened to form with a truly rectangular morphology. Under the second interpretation, our classification algorithm performs correctly, giving a false positive rate of 0%, but the model result suggests that a small percentage of rectangular networks may form in the absence of structural control. In either case, these false positive rates of 0% or ~5% do not significantly alter our results or interpretations.

Table 4
Classified Titan networks shown in color in Fig. 1 (bottom). Networks listed in bold are examples shown in Fig. 2. Network name is based on Titan SAR swath designation; the second letter differentiates networks within each swath. The lack of sequential alphanumeric designators results from the exclusion of networks of less than 10 links. Latitude and longitude coordinates are approximate network centers to the nearest degree. Apparent Shreve magnitudes are minimum values for the true Shreve magnitudes as low order tributaries cannot be detected in SAR (or likely DISR) data. The three networks without Shreve magnitudes are those for which flow direction is uncertain. The Huygens Landing Site networks do not have total lengths because projection information is not available for the mosaic used. In accordance with the original algorithm (Ichoku and Chorowicz, 1994), classification is based on the first test passed (see Section 3.3), so that tests for other categories are not administered after the first classification is made.

Network	Long.	Lat.	Classification	Apparent Shreve magnitude	Total length of network links (km)	Test(s) passed
T3 A	90°W	15°N	Dendritic	19	766	1, 2, 3
T3 B	80°W	19°N	Dendritic	15	551	1, 2, 3
T3 C	77°W	19°N	Dendritic	6	375	1, 2, 3
T28 K	263°W	74°N	Dendritic	17	261	1, 2, 3
T28 L	283°W	79°N	Dendritic	34	409	1, 2, 3
T28 N	275°W	78°N	Dendritic	10	151	1, 2, 3
T28 R	276°W	76°N	Dendritic	11	171	1, 2, 3
T28 V	259°W	75°N	Dendritic	7	40	1, 2, 3
T28 W	267°W	74°N	Dendritic	9	155	1, 2, 3
T28 X	268°W	75°N	Dendritic		355	1, 2, 3
T29 F	233°W	74°N	Dendritic	7	83	1, 2, 3
T29 H	**231°W**	**74°N**	**Dendritic**	**44**	**412**	**1, 2, 3**
T39 F	40°W	74°S	Dendritic	9	103	1, 2, 3
T7 C	**4°W**	**59°S**	**Parallel**		**1093**	**2**
T28 T	248°W	76°N	Parallel	7	73	2
T29 C(2)	**237°W**	**75°N**	**Parallel**	**8**	**60**	**2**
T29 D	**236°W**	**75°N**	**Parallel**	**12**	**99**	**3**
T7 D	7°W	55°S	Rectangular		256	1
T13 A	73°W	10°S	Rectangular	18	1122	1
T13 B	134°W	10°S	Rectangular	8	846	1
T13 C	**140°W**	**10°S**	**Rectangular**	**36**	**2455**	**1**
T13 D	86°W	11°S	Rectangular	7	364	1
T28 A	242°W	72°N	Rectangular	22	690	1
T28 I	265°W	79°N	Rectangular	9	114	1
T28 J	266°W	78°N	Rectangular	6	111	1
T28 O	269°W	77°N	Rectangular	17	292	1
T28 P	256°W	73°N	Rectangular	56	1114	1
T28 S	246°W	76°N	Rectangular	13	113	1
T28 U	276°W	77°N	Rectangular	9	201	1
T29 G	227°W	75°N	Rectangular	18	211	1
T36 A	37°W	47°S	Rectangular	10	376	1
T39 A	211°W	54°S	Rectangular	7	174	1
T39 D	57°W	86°S	Rectangular	6	325	1
T39 H	37°W	74°S	Rectangular	6	38	3
T44 B	141°W	4°S	Rectangular	10	366	1
T44 C	136°W	6°S	Rectangular	27	1130	1
T44 D	135°W	6°S	Rectangular	8	490	1
T58 A	176°W	69°S	Rectangular	10	432	3
T58 B	188°W	77°S	Rectangular	7	307	1
T58 C	248°W	78°	Rectangular	9	253	1
T59 B	**150°W**	**52°S**	**Rectangular**	**27**	**680**	**1**
T19 A	349°W	75°N	Unclassified	8	199	n/a
T28 M	280°W	80°N	Unclassified	21	193	n/a
T28 Q	276°W	76°N	Unclassified	38	337	n/a
T29 B	236°W	77°N	Unclassified	14	65	n/a
T29 C(1)	237°W	76°N	Unclassified	10	75	n/a
T29 E	234°W	75°N	Unclassified	6	40	n/a
T39 G	29°W	73°S	Unclassified	36	908	n/a
HLS A	193°W	10°S	Unclassified	27		n/a
HLS B	193°W	10°S	Rectangular	8		1
HLS C	193°W	10°S	Unclassified	7		n/a
HLS D	193°W	10°S	Rectangular	18		1

3.5. Validation of the modified algorithm using terrestrial networks

As a second and complementary approach to validating our modified algorithm, we applied our algorithm to previously classified terrestrial networks, focusing again on the predominant classification of rectangular. From the terrestrial literature cited in Section 2.2, we selected four disparate networks that have been qualitatively classified as either basic rectangular or modified rectangular (terminology from Howard, 1967). The derivation of the same classification from our modified algorithm would support the validity of our algorithm, whereas a different classification would indicate that our modifications invalidated the algorithm. A literature review of the geologic factors that control these four rectangular networks provides insight into the controls on rectangular drainage.

Our selection of rectangular networks, listed below, includes rivers on three continents and in four different climates, providing a range of conditions and having sizes comparable to both SAR and DISR networks. The networks were delineated in ArcMap on 10-m resolution National Elevation Dataset data for the United States and/or on 15-m resolution Landsat 7 images, depending on dataset availability and network visibility, with visual comparison with high-resolution (<5 m/pixel) images available in Google Earth for all networks. Network delineations were accomplished through

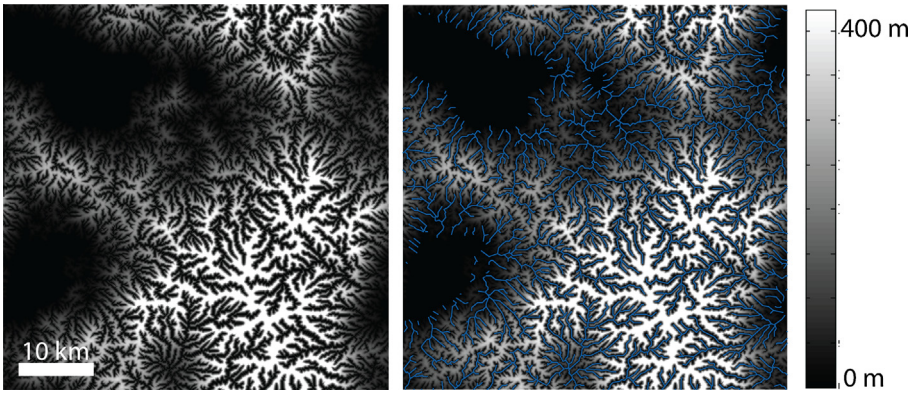

Fig. 8. One of three model landscapes we used to test our classification algorithm, showing the state of an initially undissected, randomly rough surface after 7.8 Myr of evolution. The valley networks are highlighted in blue in the right panel. Only networks containing at least ten links were used in our analysis. (For interpretation of the references to color in this figure legend, the reader is referred to the web version of this article.)

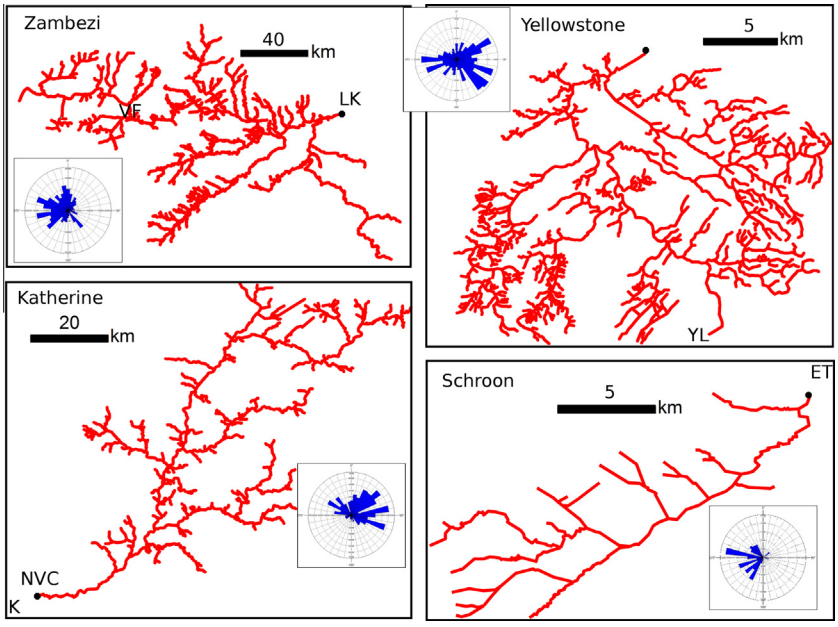

Fig. 9. Terrestrial rectangular networks analyzed in this work. The black dots show the most downstream end on the delineation of each network. Rose diagrams show the cumulative length of the links by azimuth in 10° bins and north is up in all images. On the Zambezi network, 'VF' indicates the location of Victoria Falls and 'LK' indicates Lake Kariba. On the Katherine network, 'NVC' indicates the location of the Nitmiluk Visitor Center, and 'K' signifies that the town of Katherine is ~25 km to the southwest. On the Yellowstone network, 'YL' indicates the outlet point of Yellowstone Lake. On the Schroon network, 'ET' signifies that Elizabethtown, NY, is ~5 km to the north. (For interpretation of the references to color in this figure legend, the reader is referred to the web version of this article.)

mapping and cross-checking by at least two mappers (SAD, DMB, and RC). Data for assessment of rectangularity were collected using the same tools as for the Titan networks and used in our modified algorithm.

Zambezi River (near 18°S, 26°E): The largest river system in southern Africa, the Zambezi River drains over one million square kilometers from eight different countries. Flowing from west to east, the river is divided into 3 sections (Wellington, 1955; Nugent, 1990; Moore and Larkin, 2001). The Upper Zambezi or plateau tract traverses very flat terrain underlain by Kalahari group sediments from the headwaters to the giant knickpoint known as Victoria Falls. The Middle Zambezi or trough tract flows through a major rift zone of Jurassic basalt, separated into a series of deep gorges, before emptying into Lake Kariba (part of the Gwembe Trough). Upon exiting Lake Kariba, the Lower Zambezi crosses the Mozambique coastal plain before debouching into the Indian Ocean.

The section of the Zambezi that is often used as an example of rectangular drainage (e.g., Zernitz, 1932; Howard, 1967; Twidale, 2004) is the Upper and Middle Zambezi (Fig. 9), particularly the Middle region between Victoria Falls and Lake Kariba. It is characterized by near right-angle bends and junctions between straight connecting reaches, with some sharp hairpin bends immediately downstream of Victoria Falls. Inspection of aerial images shows that the region around the Middle Zambezi is cut by obvious NW–SE and SE–NW gorges and other lineations, drainage patterns observed over 100 years ago to characterize rivers in southern Africa (Du Toit, 1910). The linear gorges are generally aligned along faults with ~50 m or vertical throw or along the shatter zones of prominent joints (Wellington, 1955; Bond, 1976).

The tectonic history of the Zambezi is complex, including processes associated with the formation and breakup of Gondwana (e.g., Stankiewicz and de Wit, 2006), but is dominated by extension. The river system is at the southern extent of the western branch of the East African Rift System (Vail, 1968). This continental rifting is a result of widespread topographic uplift (Roberts et al., 2012) and ascribed to Tertiary mantle plume activity initiated

~30–40 Myr ago (Burke, 1996; Ebinger and Sleep, 1998). Earlier Permian to Jurassic extension formed rift basins that extend from the central Kalahari NE across this region and are characterized as seismically active (Reeves, 1972, Scholz et al., 1976). In between these two events, the prior breakup of Gondwana (120–180 Myr ago) may have lead to tectonic warping of southern Africa (King, 1955). Thus, the extensional structures that control the Middle Zambezi sit within a region that was acted upon by multiple deformation events over geologic time.

Katherine River (near 13°S 133.5°E): The Katherine River has its headwaters in Nitmiluk National Park in the Northern Territory of Australia, northwest of the town of Katherine. It flows westward over the Arnhem Land plateau past the town of Katherine to its confluence with the Daly River, which then flows northward to empty into the Timor Sea. The rectangular section that we analyzed (Fig. 9) includes the region of the network on the Arnhem Land plateau with an area of ~700 km^2.

The Arnhem Land plateau is composed the Kombolgie Subgroup, a resistant Proterozoic sandstone that forms an escarpment along its contact with the underlying Precambrian sediments and intrusive rocks (Baker and Pickup, 1987). The sandstone is deformed by NW and ENE-trending rift systems inferred to have resulted from extensional tectonics during the Early Proterozoic, with some subsequent enlargement by Cretaceous-Cenozoic laterization (Needham and Stuart-Smith, 1985, Baker and Pickup, 1987, Sweet et al., 1999). River incision dated to the Miocene (Twidale, 1983) was apparently controlled by these altered joints, as mapping shows that the river follows these planes of weakness, carving deep gorges whose strikes match those of the joints (Baker and Pickup, 1987). These faults were reactivated periodically through the Middle Proterozoic (Needham and Stuart-Smith, 1985).

Yellowstone River (near 44.7°N 110.5°W): Part of the Missouri River watershed, the Yellowstone River rises near the continental divide in northwestern Wyoming, USA. It feeds Yellowstone Lake in the Yellowstone caldera, which also includes the Sour Creek and Mallard Lake resurgent domes, and then drains the lake, flowing to the northwest and then northeast. This section on the northern side of the caldera, with a series of NW–SE and SE–NW reaches (Fig. 9), has been classified as a modified rectangular ('angulate') drainage pattern.

This volcanic province is a relatively young feature in the area, with three caldera-forming eruptions in the past 2 Myr (Christiansen, 2001). Global positioning system (GPS) data show that magmatic processes continue to deform the Yellowstone caldera and surrounding plateau, producing uplift and subsidence at rates up to 15 mm/yr (Chang et al., 2007; Puskas et al., 2007). This caldera deformation is attributed to movement of magma and possibly of hydrothermal brines (Puskas et al., 2007).

The Yellowstone plateau includes the Yellowstone volcanic field and the eastern Snake River Plain, which experiences regional southwest extension across multiple late Quaternary faults (Puskas et al., 2007). These normal faults strike general NW–SE, with some orthogonal NE–SW orientations (Keefer, 1975), and merge into the northeastern boundary of the Basin and Range province. The Basin and Range province experiences east–west extension in this location (Thatcher et al., 1999; Hammond and Thatcher, 2004), producing faults that strike N–S. These two extensional stress fields overlap in this location, and the faults within the caldera show the same orientation and normal sense of motion as those on the surrounding plateau (Keefer, 1975). The orthogonal orientations of the Yellowstone Plateau and Snake River Plain, combined with the N–S orientations of the Basin and Range, correspond with those of the Yellowstone River in the area of rectangular drainage, and suggest the control on the river by these normal faults.

Schroon River (near 44.1°N 73.6°W): The Schroon River flows through the eastern Adirondack Mountains of the northeastern United States for ~100 km, terminating at the Hudson River. The rectangular section (Fig. 9) is located south of Elizabethtown, New York, and covers approximately 500 square kilometers, the smallest of these terrestrial networks and similar in size to the DISR networks.

The Adirondack region sits on the eastern edge of the North American craton. The dissected elongate dome that forms the mountains is oriented NNE–SSW with a length of 190 km and maximum topographic relief of ~1200 m. The crystalline core of the Adirondacks is comprised of metamorphic rocks deformed in the Proterozoic Grenville orogeny and dotted in structural lows by remnant Paleozoic rocks from the Taconic orogeny (Isachsen, 1975, McLelland et al., 1996).

In the eastern Adirondacks, normal faults and topographic lineaments trend NNE, parallel to the dome axis, and shift to ENE in the northern Adirondacks. Influenced by these northeasterly faults, the links of the Schroon River tend to be straight and oriented largely northeasterly, with shorter links oriented orthogonally, forming right-angle bends (Zernitz, 1932; Morisawa, 1985). The normal faults that control the rectangular drainage are ascribed both to uplift associated with delamination of overthickened crust (McLelland et al., 1996) and to orogenic compression, although a physical theory for such a mechanism was not provided (Quinn, 1933). The Adirondack Mountains may be continuing to rise tectonically, with

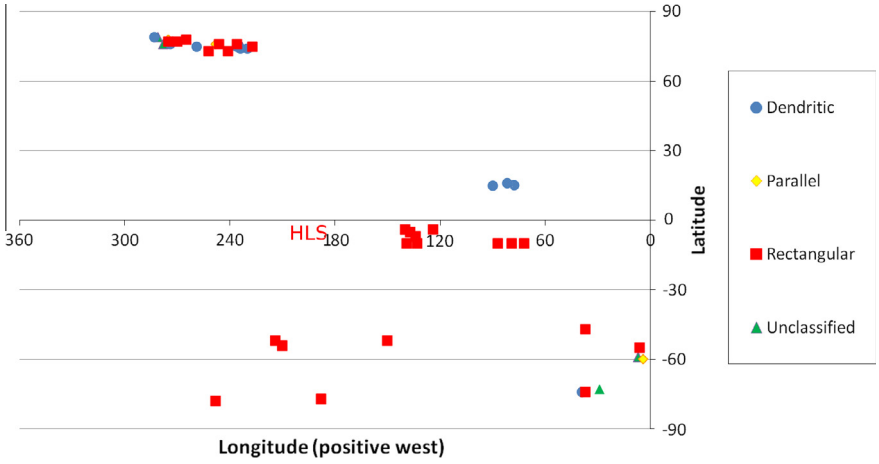

Fig. 10. Geographic distribution of networks by drainage pattern classification. Points represent the apparent centers of the networks imaged in SAR data; for indication of the extent of each network, see Fig. 1. 'HLS' shows the location of the five networks near the Huygens Landing Site imaged by DISR.

Table 5
Summary table of classifications of Titan networks, including 47 classified SAR networks and 4 classified DISR networks.

Pattern	Number	Percent
SAR Networks		
Dendritic	13	27
Parallel	4	8
Rectangular	24	50
Unclassified	7	15
DISR Networks		
Dendritic	0	0
Parallel	0	0
Rectangular	2	50
Unclassified	2	50

Table 6
Delineated fluvial feature density based on imaged area, organized by latitudinal bands of 30°.

Latitude	Delineated fluvial feature density (m/km^2)
60°–90°N	19
30°–60°N	2.5
0°–30°N	1.1
30°–0°S	3.1
60°–30°S	3.2
90°–60°S	7.1

releveling data indicating present-day movement along existing normal faults (Isachsen, 1975, see also Isachsen, 1981).

As summarized in Table 7, the three networks classified in the literature as basic rectangular were also classified by our algorithm as rectangular. For the modified rectangular ('angulate') network (the Yellowstone), our algorithm did not yield a rectangular classification. Only about one-tenth of the links of the Yellowstone River have right-angle bends (failing rectangularity test 1) and the two largest 30° bins of the trunk links are acute instead of orthogonal (failing rectangularity test 3). These trunk link orientation data are consistent with the characterization of modified rectangular networks as having acute-angle bends (Howard, 1967) and suggest overprinting of the Yellowstone/Snake River Plain fault system and the Basin and Range fault system as a cause of this network failing to meet the criteria for a rectangular classification. These results suggest that our classification approach is conservative in this regard: networks classified as rectangular by our modified algorithm are strongly rectangular; networks that have some rectangular characteristics but are not strongly rectangular may not meet the criteria for a rectangular classification.

The brief summaries above indicate that the features controlling the rectangular morphology of these four networks are tectonic in origin, including normal faults and graben (Yellowstone, Schroon, Zambezi) as well as fractures and joints (Zambezi, Katherine). Most of the controlling structures formed under regional extension, although the normal faults that control the Schroon River have been ascribed to local extension that occurred in some unknown fashion during regional contraction. The tensional stresses that formed the rest of these extensional features are attributed to a variety of mechanisms, including magmatism (Yellowstone), lithospheric processes (Schroon), and continental rifting (Zambezi, Katherine). Likewise, the timing of these mechanisms varies, with some extensional features definitely (Yellowstone) or possibly (Schroon, Zambezi) remaining active today and others being inactive (Katherine). Multiple episodes of brittle deformation have affected all of these regions during their geologic evolution.

4. Results

4.1. Titan network characteristics

4.1.1. Flow direction

Direction of flow at the network scale provides information on the direction of the slope at the time of flow. As elevation data are sparse, this indirect evidence from plan view data is useful for understanding Titan's topography at the time when the fluvial features formed. Flow directions were determined for networks that met one of three criteria – acute junction angles pointing in a consistent direction, adjacent lakes (Stofan et al., 2007), and adjacent sedimentary deposits (Jaumann et al., 2008; Lorenz et al., 2008) –, each of which indicated the downstream direction. Areas with possible distributary networks or ambiguous flow directions were marked with double-headed arrows (Fig. 1).

Results of flow direction inference in SAR data (Fig. 1, top) suggest variable controls on flow directions by region. Around the mountainous Xanadu province (centered at the equator and ~100°W longitude), acute junction angles inferred to point downstream indicate centrifugal flow around the margins of the province, consistent with previous work (Lorenz et al., 2008). Flow directions are southerly in the south with deflection to the east and west along the perimeter. The couple of northerly flow directions to the north of Xanadu are associated with Menrva Crater. At the poles, lakes provide local control as base level. In the north polar region, all delineated networks flow into the large lakes, as suggested in earlier analyses (e.g., Cartwright et al., 2011; Langhans et al., 2012). As a likely result of this control by numerous lakes, the flow directions in the north polar region appear more variable than at other latitudes. Some lacustrine control is apparent in the south polar region near Ontario Lacus (centered at 72°S and 183°W), although more distal networks do not show clear control by lakes. For the small number of analyzed networks in the southern mid-latitudes, flow is consistently southward; no networks were large enough to be analyzed in the northern mid-latitudes.

In DISR data, the general flow directions based on junction angle orientation are easterly and southerly. The dark region south of the DISR networks has been interpreted as a coastline, although it did not contain pooled liquid at the time of landing (Tomasko et al., 2005; Soderblom et al., 2007b). However, the evidence for dry lakes elsewhere on Titan (Hayes et al., 2008), including at low latitudes (Moore and Howard, 2010), supports the possibility that this equatorial dark region south of the DISR networks is a depositional setting toward which the networks drained.

4.1.2. Size statistics

For the SAR networks, a comparison was made between the network classes and network sizes quantified with apparent Shreve magnitudes and total apparent link lengths. Dendritic networks are well-integrated with a mean Shreve magnitude of 16 and a mean network summed length of 225 km (Table 8). Parallel networks are the least-integrated class with a mean Shreve magnitude of 9 and also have the lowest mean network summed length of 132 km. Rectangular networks are integrated comparably to dendritic networks with a mean Shreve magnitude of 14, but have over twice as large a mean summed length of 482 km. Unclassified networks have the highest mean magnitude of 22, and the second highest mean summed network length of 336 km.

4.1.3. Geographic distribution by type

In available SAR coverage, networks are widespread, although drainage pattern types are not equally distributed (Fig. 10). Both dendritic and parallel networks are predominantly polar. Nine of

ten dendritic networks and three of three parallel networks are located at or poleward of ~60°. In contrast, rectangular networks are more evenly distributed by number, or, if quantified by total link length, are concentrated on Xanadu in the tropics; one-third of the 26 networks (~8000 km) are located over Xanadu, one-third (~2900 km) are clustered in the north polar regions, and one-third (~2100 km) are scattered in the southern mid-latitudes and south polar region. The DISR networks, two of which are rectangular, are located in the equatorial region.

For the SAR networks, we define a parameter, "delineated fluvial feature density," as the total distance along delineated network links in bands of 30° latitude divided by the area of SAR coverage in those latitude bands. This parameter has units of length /length^2 but it differs from drainage density in two ways: (i) our delineated distance may represent river valleys instead of river channel lengths, and (ii) due to the lack of topographic information needed to define drainage basin area, our parameter normalizes total length by total imaged area within each latitudinal band instead of by drainage basin area. Because each latitudinal band likely contains both undissected regions and fluvial features that are below the detection limit of SAR data, these values for 'delineated fluvial feature density' are minima for true drainage density. Values for this parameter were calculated by summing the length of all network links (analyzed and not analyzed) in 30° latitude bands and dividing by the area of SAR coverage in those bands. The delineated fluvial feature density gives a quantitative measure by which to assess the pervasiveness of fluvial modification discernible at the resolution of the SAR data. The polar regions have the highest density and the northern mid-latitudes and tropics have the lowest (Table 6), with the difference between them greater than an order of magnitude.

4.2. Titan drainage pattern classification

Of the 48 networks in SAR data to which we applied our modified algorithm (Tables 4 and 5), 13 (27%) were classified as dendritic, implying the presence of a gentle or inconsistent slope direction at the time of drainage inception or substrate materials of homogeneous mechanical properties. Four networks (8%) are classified as parallel, implying moderate to steep slopes or the presence of parallel, elongate landforms. Twenty-four networks (50%) are classified by the modified algorithm as rectangular. Seven networks (15%) fall into the "unclassified" category. Of the four networks analyzed at the Huygens landing site, networks B and D are classified as rectangular, with network D having the stronger rectangularity (passing the first rectangular test with the higher percentage of right angle bends); networks A and C are unclassified (Tables 4 and 5, Fig. 3).

Based on our statistical analysis (Section 3.3) we did not classify networks with fewer than 10 links. However, these networks are not insignificant (Fig. 1, bottom), as small networks and individual features account for ~73,300 km of total length, compared to the analyzed networks which total only ~19,400 km in length. The combined total length of delineated networks, both analyzed and not analyzed, is thus ~92,700 km. This value for all delineated networks is approximately four times the combined length reported in the most recent previous global mapping effort with a combined dataset of networks as delineated on SAR swaths up through T57, on VIMS data up through T48, on ISS data through T0, and in DISR data (Langhans et al., 2012). The disparity of datasets on which the networks were delineated may be one cause for the discrepancy, as may the difference in the latitudinal coverage of the two studies. Langhans et al. (2012) indicate that another cause may be that their value "is certainly underestimated due to the incomplete coverage and the segmented storage of valleys in the database."

5. Discussion

5.1. Geologic implications of rectangular terrestrial drainage networks

Although the mechanisms that produce the structures that control the four terrestrial rectangular networks vary, the structures themselves are uniformly extensional, and possibly developed through multiple episodes of deformation. Characteristics of rectangular networks, most notably right angle bends, can also result from the influence of structures formed by stresses other than regional extension. Offset drainage across a strike-slip fault, such as Wallace Creek (Sieh and Jahns, 1984) and Little Rock Creek (Morisawa, 1985) along the San Andreas Fault, form well-defined right-angle bends at the intersection of the river valley and fault. However, rivers offset along strike-slip faults form orthogonal bends only within the strike-slip zone; unless affected by other directional biases in the substrate, these networks would likely not display the necessary proportions of right angle bends to be classified as rectangular.

Other sources of directional bias are also possible. Geologic fabric (e.g., cleavage, bedding) may also influence drainage patterns, although the effect of that influence is variable (Hodgkinson et al., 2006) and not documented in the terrestrial rectangular networks analyze here. Fossil linear dune fields could impart a linear (and possibly rectilinear) morphology to drainage, as could tilting and erosion of stratified crustal blocks. On Earth, however, the elongate nature of these blocks typically imparts a trellis-type morphology to drainage (Fig. 11), and we suspect that a similar morphology would develop on fossil linear dunes for a similar reason. Headward migration, especially over an initial planar sloping topography, may create networks with qualitatively orthogonal junction angles (Howard, 1994; Foster and Kelsey, 2012), although these elongate, parallel drainages likewise appear more similar to

Table 8
Mean apparent Shreve magnitudes and mean summed network link lengths for each network class. The unclassified networks have the largest apparent Shreve magnitude, suggesting that the lack of classification results from a variety of drainage patterns integrated into a single network.

Classification	Mean Shreve magnitude	Mean summed link length (km)
Dendritic	16	225
Parallel	9	132
Rectangular	14	482
Unclassified	22	336

Table 7
Terrestrial networks classified in the literature as rectangular, used for testing our modified algorithm for a false negative rate for rectangularity and for assessing likely causes for rectangularity.

Network	Location	Qualitative classification	Rectangular test passed
Katherine	13°S 133.5°E	Rectangular	1
Zambezi	18°S, 26°E	Rectangular	1
Yellowstone	44.7°N 110.5°W	Modified Rectangular	Did not pass
Schroon	44.1°N 73.6°W	Rectangular	2

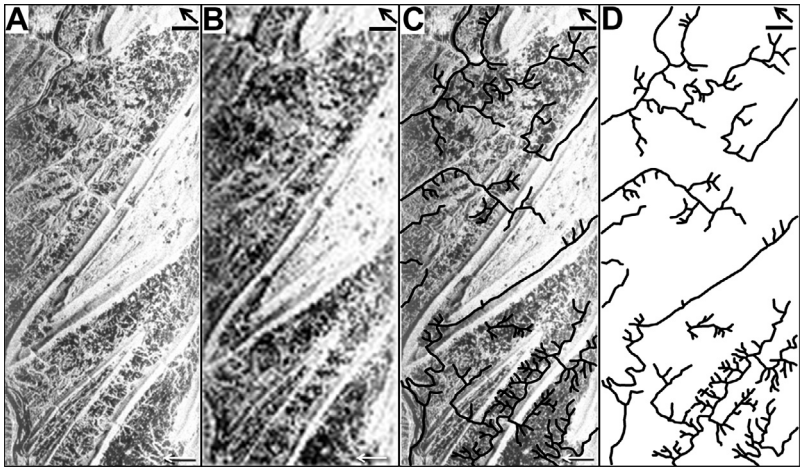

Fig. 11. AIRSAR survey data over the Middle Susquehanna River, Pennsylvania, centered at 40.8°N 76.6°W, showing typical valley and ridge topography, with bright slopes facing the radar (i.e., to the SE) and darker slope facing away from the radar. (A) Raw data, resolution 100 m/pixel. (B) Data degraded to best Titan SAR resolution of 350 m/pixel. (C) Delineation of Susquehanna tributaries over raw AIRSAR data. Tributaries can be seen in some places cross-cutting ridges. (D) Delineation of Susquehanna tributaries. On all images, black arrows point north, black scale bars equal 3 km, and radar illumination direction is from the right.

trellis than to rectangular networks. A more equant rectilinear drainage pattern could develop on polygonal cracks such as result from shrinkage during cooling of either silicate or icy (cryo)lavas or desiccation of sediments. However, the internal angles of such shrinkage polygons tend towards 60° instead of the right-angle bends characteristic of rectangular networks, leaving the development of right-angle bends not easily accounted for in this scenario.

Regionally extensive right angle bends are documented to have developed in response to compressional stress. Orthogonal joints sets formed in the Catskill Delta of central New York during the Alleghanian orogeny (Engelder, 1985; Engelder and Oertel, 1985). Opening mode 'cross-fold joints' formed from elevated pore fluid pressure caused by regional compression. Subsequent 'strike joints' formed during uplift and relaxation along preexisting (compressional) structures. In Zimbabwe, conjugate faults propagated across an area of regional compression (Fedo et al., 1995). The faulting followed plutonism and was followed in turn by magmatic filling of the fractures, suggesting the plutonism to be a possible cause for the faulting, but no mechanism was suggested in the original work.

Thus, compression may create regional networks of orthogonal structures, and it seems possible that these structures may in turn lead to formation of rectangular drainage. However, we are not aware of regionally extensive rectangular river networks documented at these cited locations. In the four widely documented examples of rectangular drainage analyzed in Section 4.6 above, the controlling structures were extensional and were formed during regional extension, not regional compression. We conclude that, although some control by orthogonal structures arising from regional compression is possible, terrestrial rectangular networks are typically controlled by extensional structures that formed during regional extension.

5.2. Geologic implications of rectangular drainage networks on Titan

As set out in the above discussion, extensional tectonism appears to be the most effective mechanism for producing the regional directional biases in crustal material strength properties that result in rectangular networks on Earth. At Titan surface temperatures (~94 K), the response to stress of cryogenic ice is thought to be similar to that of silicate crust on Earth, so that brittle deformation of the Titan crust is expected (Collins et al., 2010). Tectonic deformation of outer Solar System satellites is widespread, resulting from stresses due to orbital dynamics and changes in the hydrostatic equilibrium shape (Collins et al., 2010). Given the available energy for tectonic deformation and the similar brittle response to tectonic stresses of rock and cryogenic ice, the mechanism of extensional tectonism is also possible on Titan. In view of the unlikelihood of other sources of directional bias producing regional rectangular drainages and of the demonstrated effectiveness of extensional tectonism on Earth for producing rectangular networks, we infer that extensional tectonism on Titan is the most likely mechanism for producing rectangular networks on Titan.

That rectangular networks comprise more than half of the large-scale networks analyzed in this study contrasts with the results of a previous morphologic classification, in which dendritic networks were given as the most numerous class (10 of 23 fluvial networks classified, or 43%; Langhans et al., 2012). Other workers have also reported dendritic networks as being predominant in Xanadu (Lorenz et al., 2008), the north pole (Stofan et al., 2007; Cartwright et al., 2011), and the Huygens landing site (Tomasko et al., 2005; Soderblom et al., 2007a), where this study finds predominantly, although not exclusively, rectangular morphologies (Fig. 1). In these previous works, the geomorphic term 'dendritic' may have substituted for the more generic term, 'branched.' Although networks in any medium may be generically referred to as 'dendritic,' dendritic drainage networks have both specific criteria and specific geologic implications (Table 1). Analysis here shows that networks at Xanadu, in the north polar region and at the Huygens Landing site tend to have rectangular instead of dendritic morphologies (Fig. 1 bottom, and Fig. 3).

In comparison to the more limited geographic distribution of other network types, the wider geographic distribution of rectangular networks indicates that the geologic controls promoting rectangular networks, such as faults, fractures or joints, are widespread on Titan's surface. The finding of rectangular networks in both SAR and DISR data suggests that these geologic controls are also effective over areas ranging in size from the Huygens landing site to Xanadu. However, most of the delineated fluvial features were not sufficiently integrated in available data to be considered for classification analysis (Fig. 1, bottom). While this apparent lack of integration may be in part a function of low image resolution, fluvial networks on Titan may in actuality be poorly integrated, due either to hypothesized karst-like dissolution processes (e.g., Mitchell and Malask, 2011) or to difficulties eroding the substrate (Collins et al., 2012; Litwin et al., 2012).

5.3. Consideration of trellis classification

Like rectangular networks, trellis networks are rectilinear drainages that feature straight links and near-right angle bends. In the original algorithm by Ichoku and Chorowicz (1994), rectangularity (see tests for rectangularity in Section 3.3 above) is required for rectangular networks and is a possible (though not required) attribute of trellis networks (Fig. 5). The original algorithm indicates that the first attribute for distinguishing between trellis and rectangular networks is the mean exterior link length, which is shorter for trellis than for rectangular networks. Due to the low resolution of the Titan data, we cannot discern true external links (as demonstrated by the non-visibility of the DISR networks in the SAR data; Soderblom et al., 2007a), so cannot accurately assess this attribute, relying instead on apparent external links. Thus, there may be trellis networks on Titan that have been misclassified as rectangular.

To test for possible misclassifications of trellis networks as rectangular, we inspected AIRSAR data to assess if the appearance of a typical landscape that hosts terrestrial trellis networks is comparable to the appearance of the landscapes that host rectangular networks on Titan. Terrestrial trellis networks form in areas of folded, layered sedimentary rocks of varying resistance, whose erosion creates alternating, elongate valleys and ridges. Trunk channels of fluvial networks flow along these valleys and are fed by smaller tributaries, which either cut across the ridges or are sourced from the ridge slopes. The Valley and Ridge physiographic province in the eastern US (Ritter et al., 2002) is an illustration of this morphology and its resultant trellis drainage. In AIRSAR data over the Susquehanna River of the Valley and Ridge province in central Pennsylvania, USA, the topography creates bright slopes resulting from illumination by the radar and darker slopes which face away from the radar (Fig. 11). We inspected the areas immediately surrounding each Titan network classified as rectangular for evidence of similar alternating, linear, radar-bright and radar-dark patterns indicative of valleys and ridges or large folds. None of the regions that host the 26 rectangular networks seen in SAR data showed a radar return pattern that was convincingly consistent with valley and ridge topography, the alternating linear valleys and ridges that provide the setting for the development of trellis networks. Thus, we consider it unlikely that the classified rectangular networks are actually trellis networks.

5.4. Implications of other Titan network characteristics

5.4.1. Flow directions

The disparate flow directions at the poles and general termination of north polar networks into lakes indicate that the lakes, serving as base level for these networks, influence the network flow directions, or that the pre-existing topography that led to lake formation also shaped the region's drainage networks. Around Xanadu, flow directions indicate regional control on flow by the (paleo)topography. Centripetal flow, recorded most clearly in fluvial networks along the southern margins of Xanadu (Fig. 1), indicates that it was a topographic high, possibly a plateau, at the time these networks formed. The region is currently low compared to the surrounding terrain (Stiles et al., 2009; Zebker et al., 2009), hypothesized to have resulted from regional subsidence due to crustal extension, which may also account for the rectilinear river valleys (Radebaugh et al., 2011). This comparison suggests that some valley networks on Titan (e.g., around southern Xanadu) are relict, although the sparseness of the SARtopo data (Stiles et al., 2009) and the low resolution of the altimetry data (Zebker et al., 2009) make a definitive statement difficult. In contrast, the southerly flow directions derived from plan view morphology of the DISR networks are consistent with current topography derived from stereo DISR images, showing the dissected uplands a few hundred meters above the flatter baselevel (Tomasko et al., 2005; Soderblom et al., 2007a).

5.4.2. Geographic distribution by type

The geographic clustering of the networks as shown by the delineated fluvial features density indicates that fluvial activity is more geomorphologically effective at certain latitudes on Titan. This enhanced effectiveness could be due to either greater atmospheric influence or less surface/subsurface resistance. Atmospheric patterns may produce heavier or more consistent precipitation in some latitudinal bands compared to others, as suggested by precipitation modeling (e.g., Schneider et al., 2012). Clouds have been observed over the south pole during the southern summer with hourly variation (Atreya et al., 2009), similar to rainstorms on Earth. Similar phenomena were observed at low latitudes but with only temporary surface change (Turtle et al., 2011), which is not yet well-understood. Surface/subsurface effects that may facilitate formation of fluvial networks might include greater availability of sediment appropriately sized for fluvial transport or greater concentrations of tectonic structures.

5.4.3. Size statistics

The Titan rectangular networks imaged in SAR data are integrated comparably to the other network classes, with a mean Shreve magnitude approximately equal to that of the dendritic networks, but they have the greatest mean summed link length (the total length of all the network links divided by the number of networks for each class) of the four classes, twice as great as that of the dendritic networks (Table 8). The cause for this maximum total link length may be indicated by laboratory experimental results on abrasion resistance of cryogenic ice, for which the very slow rate of erosion suggests that, to be geomorphically effective, fluvial erosion on Titan must occur in previously comminuted or pre-fractured bedrock (Litwin et al., 2012; Collins et al., 2012). Because rectangular networks imply control by weaknesses or biases in substrate strength, our finding that rectangular networks have greater total link lengths than the other networks without such control is consistent with the idea that Titan rivers erode significantly more readily along pre-existing weaknesses.

The statistics indicate that parallel networks are poorly developed and poorly integrated. The lowest mean Shreve magnitude for these networks (Table 8) may be expected from the network topology: parallel tributaries form fewer junctions than more orthogonal tributaries. The reason for the lowest mean network summed link length is uncertain, but suggests that the areas where parallel networks are found on Titan experience less erosion, resulting in less incision and shorter links. Such a scenario might occur where the moderate to steeply sloping surfaces, which commonly experience more parallel drainage (cf., Howard, 1967) and would otherwise be expected to experience more erosion than shallowly sloping surfaces, are preferentially composed of bedrock or only thin alluvium.

The unclassified networks have the largest mean Shreve magnitude (Table 8), which lends support to the idea that this classification is due to large networks with sub-basins of different network morphologies (Ichoku and Chorowicz, 1994). Subdividing networks into homogeneous subnetworks requires recognizing *a priori* the patterns of different parts of a network. Based on experience, intelligent guesses can be made to speed up this process, although the original (automated) approach for accomplishing this subdivision was simply to divide large networks into smaller ones, which would necessarily tend to relatively greater homogeneity, and therefore be more readily classifiable (Ichoku and Chorowicz, 1994, p. 164). Based on the identification here of large unclassified networks, future work can focus on such subnetwork division and classification.

6. Conclusions and future work

The widespread distribution of rectangular fluvial networks on Titan provides evidence for widespread fracturing and/or faulting of Titan's crust. Tectonism may be an important resurfacing mechanism for Titan's lightly cratered surface, consistent with the apparently limited fluvial exhumation of the current surface (Black et al., 2012). Extensional tectonism is pervasive on icy satellites in the outer Solar System (Collins et al., 2010). Previous modeling work indicates that long-term cooling of Titan would have led to for contractional tectonism (e.g., Mitri et al., 2010). Given the resolution limitations of the SAR data, it is possible that some of our classified rectangular networks are actually trellis networks. However, based on comparison in SAR data of a terrestrial landscape with trellis drainage to each of the Titan landscapes with rectangular drainage, we conclude that any such misclassifications are unlikely or few in number. Previous image analysis led to the hypothesis of contraction and extension over Xanadu (Radebaugh et al., 2011). Our findings provide evidence of more globally distributed extensional stresses. Both regional tension and regional compression have been shown to generate nearly orthogonal fault or joint patterns on Earth, but the prominent examples of terrestrial rectangular drainage networks analyzed here are associated with regional extension. Thus, we consider distributed extension to be the most likely explanation for Titan's rectangular drainages.

If the inferred rectangular networks are controlled by extensional structures, then the orientations of the network links (e.g., Fig. 1, rose diagrams) contain information about the orientations of the tectonic stresses that created those controlling structures. Accessing this information is complicated by the resolution of the SAR data, which limits the discernible extent of the network. Similarly, the topographic fabric surrounding the rectangular networks, which might serve as additional data of structural orientations, is likely muted by tholin deposition from the atmosphere. To the extent that the rectangular networks reflect the underlying extensional structures, their expression of tectonic extension is strikingly different from the expression of large extensional strains on other large icy satellites, such as the bands on Europa or the grooved terrain on Ganymede.

Because the resolution and noise level of the SAR data limit our ability to resolve small fluvial features, our conclusions about the relative frequencies of different network morphologies are based on only the largest fluvial networks, which constitute a minority of the known fluvial networks (Fig. 1, bottom). Thus, these relative frequencies could change with a more complete and detailed view of Titan's surface. Available SAR data processed with improved denoising techniques (e.g., Lucas et al., 2011, 2012) may allow for more extensive and better network delineations, which would result in more and more reliable classifications. Network delineation and analysis on upcoming Cassini SAR data would likely also increase the number and geospatial distribution of classified networks, which may change the measured distribution of network morphologies. Higher-resolution data from an aircraft on Titan (e.g., Barnes et al., 2011) would further enable testing and extension of our results.

Comparison of other data would also help test our results. Favorable comparison among link orientations of different networks or among link orientations and other hypothesized tectonic structures such as mountain chains (Radebaugh et al., 2007) and unit contacts (Radebaugh et al., 2011) would support an inference of local or regional tectonic control. A lack of coincidence between dominant azimuths from fluvial networks and the orientations of hypothesized tectonic structures would suggest either that the fluvial networks are not structurally controlled, in contradiction to the conclusion drawn here, or that the networks and the other structures formed at different times. Either result would contribute to a better understanding of the interplay of hydrocarbon rivers with Titan's icy surface.

Acknowledgments

This work was enabled by support from NASA Cassini Data Analysis Program Grant NNX08BA81G to DMB. The funding source had no involvement in this research. We thank Joshua Emery and Robert D. Hatcher, Jr., for their input on a nascent version of this work (Drummond, 2012), and Joshua Emery for his assistance with the statistical analysis. We thank Trent Hare for his help with the ArcGIS files.

References

Atreya, S.K. et al., 2009. Volatile origin and cycles: Nitrogen and methane. In: Brown, R.H., Lebreton, J., Waite, J.H. (Eds.), Titan from Cassini–Huygens. Springer, Dordrecht, pp. 177–199.
Baker, V.R., Pickup, G., 1987. Flood geomorphology of the Katherine Gorge, Northern Territory, Australia. Geol. Soc. Am. Bull. 98, 635–646.
Barnes, J.W. et al., 2007. Near-infrared spectral mapping of Titan's mountains and channels. J. Geophys. Res. 112, E11006. http://dx.doi.org/10.1029/2007JE002932.
Barnes, J.W. et al., 2008. Spectroscopy, morphometry, and photoclinometry of Titan's dunefields from Cassini/VIMS. Icarus 195, 400–414.
Barnes, J.W. et al., 2011. AVIATR—Aerial vehicle for in situ and airborne Titan reconnaissance: A Titan airplane mission concept. Exp. Astron. http://dx.doi.org/10.1007/s10686011-9275-9.
Baugh, N.F., 2008. Fluvial Channels on Titan. Master's thesis. University of Arizona.
Black, B.A., Perron, J.T., Burr, D.M., Drummond, S.A., 2012. Estimating erosional exhumation on Titan from drainage network morphology. J. Geophys. Res. http://dx.doi.org/10.1029/2012JE004085.
Bond, G., 1976. The geology and formation of the Victoria Falls. In: Phillipson, D.W. (Ed.), Mosi- ou-Tunya: A Handbook to the Victoria Falls region. Longmans, London, pp. 19–27.
Brown, R.H. et al., 2004. The Cassini Visual and Infrared Mapping Spectrometer (VIMS) investigation. Space Sci. Rev. 115, 111–168.
Brown, R.H., Barnes, J.W., Melosh, H.J., 2011. On Titan's Xanadu region. Icarus 214, 556–560. http://dx.doi.org/10.1016/j.icarus.2011.03.018.
Burberry, C.M., Cosgrove, J.W., Liu, J.G., 2008. Spatial arrangement of fold types in the Zagros Simply Folded Belt, Iran, indicated by landform morphology and drainage pattern characteristics. J. Maps, 417–430.
Burke, K., 1996. The African plate. S. Afr. J. Geol. 99, 339–409.
Burr, D.M. et al., 2009. Fluvial network analysis on Titan: Evidence for subsurface structure and west-to-east wind flow, southwestern Xanadu. Geophys. Res. Lett. 36, L22203. http://dx.doi.org/10.1029/2009GL040909.
Burr, D.M. et al., 2012. Fluvial features on Titan: Insights from morphology and modeling. Geol. Soc. Am. Bull. http://dx.doi.org/10.1130/B30612.1.
Cartwright, R., Clayton, J.A., Kirk, R.L., 2011. Channel morphometry, sediment transport, and implications for tectonic activity and surficial ages of Titan basins. Icarus 214, 561–570.
Chang, W.-L., Smith, R.B., Wicks, C., Farrell, J.M., Puskas, C.M., 2007. Intrusion of the Yellowstone Caldera, 2004 to 2006. Science 318, 952–956. http://dx.doi.org/10.1126/science.1146842.
Christiansen, R.L., 2001. The Quaternary and Pliocene Yellowstone Plateau Volcanic Field of Wyoming, Idaho, and Montana. USGS Professional Paper 729-G.
Collins, G.C., 2005. Relative rates of fluvial bedrock incision on Titan and Earth. Geophys. Res. Lett. 32, L22202. http://dx.doi.org/10.1029/2005GL024551.
Collins, G.C. et al., 2010. Tectonics of the outer planet satellites. In: Watters, T.D., Schultz, R.A. (Eds.), Planetary Tectonics. Cambridge University Press, Cambridge, pp. 264–350.
Collins, G.C., Sklar, L.S., Litwin, K.L., Polito, P.J., 2012. Do Titan's river channels carve into ice bedrock or loose regolith? In: Cottini, V., Nixon, C., Lorenz, R. (Eds.), Titan through Time, NASA Goddard Space Flight Center, April 3–5. p. 30. <http://spacescience.arc.nasa.gov/events/titan-through-time-ii-workshop>.
D'Alessandro, Miccadei, E., Piacentini, T., 2008. Morphotectonic study of the lower Sangro River valley (Abruzzi, Central Italy). Geomorphology 102(1), 145–158. http://dx.doi.org/10.1016/j.geomorph.2007.06.019.
Drummond, S.A., 2012. Structural Control of Fluvial Network Morphology on Titan. MS Thesis, University of Tennessee Knoxville.
Du Toit, A.L., 1910. The evolution of the river system of Griqualand West. Trans. R. Soc. S. Afr. 1, 347–361.
Ebinger, C.J., Sleep, N., 1998. Cenozoic magmatism throughout East Africa resulting from impact of a single plume. Nature 395, 788–791.
Elachi, C. et al., 2005. Cassini Radar views the surface of Titan. Science 308, 970–974. http://dx.doi.org/10.1126/science.1109919.
Engelder, T., 1985. Loading paths to joint propagation during a tectonic cycle: Example from the Appalachian Plateau, USA. J. Struct. Geol. 7, 459–476.

Engelder, T., Oertel, G., 1985. The correlation between undercompaction and tectonic jointing within the Devonian Catskill Delta. Geology 13, 863–866.
Eyles, N., Arnaud, E., Scheidegger, A.E., Eyles, C.H., 1997. Bedrock jointing and geomorphology in southwestern Ontario, Canada: An example of tectonic predesign. Geomorphology 19, 17–34.
Fedo, C.M., Eriksson, K.A., Blenkinsop, T.G., 1995. Geologic history of the Archean Buhwa Greenstone Belt and surrounding granite – gneiss terrane, Zimbabwe, with implications for the evolution of the Limpopo Belt. Can. J. Earth Sci. 32, 1977–1990.
Foster, M.A., Kelsey, H.M., 2012. Knickpoint and knickzone formation and propagation, South Fork Eel River, northern California. Geosphere 8, 403–416. http://dx.doi.org/10.1130/GES00700.1.
Griffith, C., Hall, J., Geballe, T., 2000. Detection of daily clouds on Titan. Science 290, 509–513.
Gupta, S., 1997. Himalayan drainage patterns and the origin of fluvial megafans in the Ganges foreland basin. Geology 25 (1), 11–14.
Hammond, W.C., Thatcher, W., 2004. Contemporary tectonic deformation of the Basin and Range province, western United States: 10 years of observation with the Global Positioning System. J. Geophys. Res. 109, B08403. http://dx.doi.org/10.1029/2003JB002746.
Hayes, A. et al., 2008. Hydrocarbon lakes on Titan: Distribution and interaction with a porous regolith. Geophys. Res. Lett. 35, L09204. http://dx.doi.org/10.1029/2008GL033409.
Hodgkinson, J.H., McLoughlin, S., Cox, M., 2006. The influence of geological fabric and scale on drainage pattern analysis in a catchment of metamorphic terrain: Laceys Creek, southeast Queensland, Australia. Geomorphology 81, 394–407. http://dx.doi.org/10.1016/j.geomorph.2006.04.019.
Howard, A.D., 1967. Drainage analysis in geologic interpretation: A summation. AAPG Bull. 51, 2246–2259.
Howard, A.D., 1994. A detachment-limited model of drainage basin evolution. Water Resour. Res. 30 (7), 2261–2285.
Ichoku, C., Chorowicz, J., 1994. A numerical approach to the analysis and classification of channel network patterns. Water Resour. Res. 30 (2), 161–174.
Isachsen, Y.W., 1975. Possible evidence for contemporary doming of the Adirondack Mountains, New York, and suggested implications for regional tectonics and seismicity. Tectonophysics 29, 169–181.
Isachsen, Y.W., 1981. Contemporary doming of the Adirondack Mountains: Further evidence from releveling. Tectonophysics 71, 95–96.
Jaumann, R. et al., 2008. Fluvial erosion and post-erosional processes on Titan. Icarus 197, 526–538.
Jaumann, R. et al., 2009. Geology and surface processes on Titan. In: Brown, R.H., Lebreton, J., Waite, J.H. (Eds.), Titan from Cassini–Huygens. Springer, Dordrecht, pp. 75–140.
Keefer, W.R., 1975. The Geologic Story of Yellowstone National Park, U.S. Geological Survey Bulletin 1347.
King, L.C., 1955. Pediplanation and isostacy: An example from South Africa. Q. J. Geol. Soc. Lond. 111, 353–359.
Lamb, M.P., Howard, A.D., Johnson, J., Whipple, K.X., Dietrich, W.E., Perron, J.T., 2006. Can springs cut canyons into rock? J. Geophys. Res. 111, E07002. http://dx.doi.org/10.1029/2005JE002663.
Lamb, M., Dietrich, W., Aciego, S., DePaolo, D., Manga, M., 2008. Formation of Box Canyon, Idaho, by megaflood: Implications for seepage erosion on Earth and Mars. Science 320 (5879), 1067–1070.
Langhans, M.H. et al., 2012. Titan's fluvial valleys: Morphology, distribution, and spectral properties. Planet. Space Sci. 60 (1), 34–51.
LeGall, A., Janssen, M.A., Paillou, P., Lorenz, R.D., Wall, S.D.the Cassini Radar Team, 2010. Radar-bright channels on Titan. Icarus 207, 948–958.
Litwin, K.L., Zygielbaum, B.R., Polito, P.J., Sklar, L.S., Collins, G.C., 2012. Influence of temperature, composition and grain size on the tensile failure of water ice: Implications for erosion on Titan. J. Geophys. Res. – Planets 117, E08013, http://dx.doi.org/10.1029/2012JE004101.
Lopes, R.M.C. et al., 2007. Cryovolcanic features on Titan's surface as revealed by the Cassini Titan Radar Mapper. Icarus 186, 395–412.
Lopes, R.M.C. et al., 2010. Distribution and interplay of geologic processes on Titan from Cassini radar data. Icarus 205, 540–558.
Lorenz, R.D. et al., 2007. Titan's young surface: Initial crater survey by Cassini RADAR and model comparison. Geophys. Res. Lett. 34, L07204. http://dx.doi.org/10.1029/2006GL028971.
Lorenz, R.D. et al., 2008. Fluvial channels on Titan: Initial Cassini RADAR observations. Planet. Space Sci. 56, 1132–1144.
Lucas, A., Aharonson, O., Hayes, A.G., Deledalle, C.A., Kirk, R.L., 2011. Enhanced Processing and Analysis of Cassini SAR Images of Titan. American Geophysical Union Fall Meeting 2011, P33E-1795.
Lucas, A. et al., 2012. Clues to Titan hydrology from enhanced SAR image processing. Lunar Planet. Sci. Conf. 43, 2566.
Lunine, J.I., Atreya, S.K., 2008. The methane cycle on Titan. Nat. Geosci. 1, 159–164.
McLelland, J., Daly, J.S., McLelland., J. 1996. The Grenville Orogenic Cycle (ca. 1350–1000 Ma): an Adirondack perspective. Tectonophysics 265 (1–2) 1–28. http:dx.doi.org/10.1016/S0040-1951(96)00144-8.
Mejía, A.I., Niemann, J.D., 2008. Identification and characterization of dendritic, parallel, pinnate, rectangular, and trellis networks based on deviations from planform self similarity. J. Geophys. Res. 113, F02015. http://dx.doi.org/10.1029/2007JF000781.
Mitchell, K.L., Malask, M., 2011. Karst on Titan. First International Planetary Caves Workshop: Implications for Astrobiology, Climate, Detection, and Exploration, held October 25–28, 2011 in Carlsbad, New Mexico. LPI Contribution No. 1640, p. 18.
Mitri, G., Showman, A.P., Lunine, J.I., Lorenz, R.D., 2007. Hydrocarbon lakes on Titan. Icarus 186, 385–394.
Mitri, G. et al., 2010. Mountains on Titan: Modeling and observations. J. Geophys. Res. 115, E10002. http://dx.doi.org/10.1029/2010JE003592.
Moore, J.M., Howard, A.D., 2010. Are the basins of Titan's Hotei Regio and Tui Regio sites of former low latitude seas? Geophys. Res. Lett. 37 (22), L22205. http://dx.doi.org/10.1029/2010GL045234.
Moore, A.E., Larkin, P.A., 2001. Drainage evolution in southcentral Africa since the breakup of Gondwana. S. Afr. J. Geol. 104, 47–68.
Moore, J.M., Pappalardo, R.T., 2011. Titan: An exogenic world? Icarus 212, 790–806.
Morisawa, M., 1985. Rivers: Form and Process. Longman, London, 222p.
Needham, R.S., Stuart-Smith, P.G., 1985. Stratigraphy and tectonics of the Early to Middle Proterozoic transition, Katherine-El Sherana area, Northern Territory. Aust. J. Earth Sci: Int. Geosci. J. Geol. Soc. Aust. 32 (2), 219–230.
Neish, C.D., Lorenz, R.D., 2012. Titan's global crater population: A new assessment. Planet. Space Sci. 60, 26–33.
Nugent, C., 1990. The Zambezi River: Tectonism, climatic change and drainage evolution: Palaeogeography. Palaeoclimatol. Palaeoecol. 78 (1–2), 55–69. http://dx.doi.org/10.1016/0031-0182(90)90204-k.
Perron, J.T., Lamb, M.P., Koven, C.D., Fung, I.Y., Yager, E., Adámkovics, M., 2006. Valley formation on Titan. J. Geophys. Res. 111, E11001. http://dx.doi.org/10.1029/2005JE002602.
Porco, C.C. et al., 2005. Imaging of Titan from the Cassini spacecraft. Nature 434, 159–168.
Puskas, C.M., Smith, R.B., Meertens, C.M., Chang, W.L., 2007. Crustal deformation of the Yellowstone–Snake River Plain volcano-tectonic system: Campaign and continuous GPS observations, 1987–2004. J. Geophys. Res. 112, B03401, http://dx.doi.org/10.1029/2006JB004325.
Quinn, A., 1933. Normal faults of the Lake Champlain region. J. Geology 41, 113–143.
Radebaugh, J. et al., 2007. Mountains on Titan observed by Cassini Radar. Icarus 192, 77–91.
Radebaugh, J. et al., 2008. Dunes on Titan observed by Cassini Radar. Icarus 194, 690–703.
Radebaugh, J. et al., 2011. Regional geomorphology and history of Titan's Xanadu province. Icarus 211, 672–685.
Reeves, C.V., 1972. Rifting in the Kalahari? Nature 237, 95–96.
Ribolini, A., Spagnolo, M., 2007. Drainage network geometry versus tectonics in the Argentera Massif (French–Italian Alps). Geomorphology 93, 253–266.
Ritter, D.F., Kochel, R.C., Miller, J.R., 2002. Process Geomorphology. Waveland Press, Long Grove, IL.
Roberts, E.M. et al., 2012. Initiation of the western branch of the East African Rift coeval with the eastern branch. Nat. Geosci. 5 (4), 289–294.
Schneider, T., Graves, S.D.B., Schaller, E.L., Brown, M.E., 2012. Polar methane accumulation and rainstorms on Titan from simulations of the methane cycle. Nat. Lett. http://dx.doi.org/10.1038/nature10666.
Scholz, C.H., Koczynski, T.A., Hutchins, D.G., 1976. Evidence for incipient rifting in Southern Africa. Geophys. J. Int. 44 (1), 135–144. http://dx.doi.org/10.1111/j.1365-246X.1976.tb00278.
Sharma, B.K., Bhola, A.M., Scheidegger, A.E., 2003. Neotectonic activity in the Chamba Nappe of the Himachal Himalaya: Jointing control of the drainage patterns. J. Geol. Soc. India 1, 159–169.
Sieh, K.E., Jahns, R.H., 1984. Holocene activity of the San Andreas fault at Wallace Creek, California. GSA Bull. 95, 883–896.
Soderblom, L.A. et al., 2007a. Topography and geomorphology of the Huygens landing site on Titan. Planet. Space Sci. 55, 2015–2024.
Soderblom, L.A. et al., 2007b. Correlations between Cassini VIMS spectra and RADAR SAR images: Implications for Titan's surface composition and the character of the Huygens Probe Landing Site. Planet. Space Sci. 55, 2025–2036.
Sotin, C. et al., 2005. Release of volatiles from a possible cryovolcano from near-infrared imaging of Titan. Nature 435, 786–789.
Stankiewicz, J., de Wit, M.J., 2006. A proposed drainage evolution model for Central Africa—Did the Congo flow east? J. Afr. Earth Sci. 44, 75–84.
Stiles, B.W. et al., 2009. Determining Titan surface topography from Cassini SAR data. Icarus 202 (2), 584–598.
Stofan, E.R. et al., 2007. The lakes of Titan. Nature 445 (4), 61–64.
Sweet, I.P., Brakel, A.T., Carson, L., 1999. The Kombolgie Subgroup - a new look at an old 'formation'. AGSO Research Newsletter 30, 26–28.
Thatcher, W., Foulger, G.R., Julian, B.R., Svarc, J., Quilty, E., Bawden, G.W., 1999. Present day deformation across the Basin and Range province, western United States. Science 282, 1714–1718.
Thornbury, W.D., 1954. Principles of Geomorphology. Wiley, New York, 594p.
Tomasko, M.G. et al., 2005. Rain, winds and haze during the Huygens probe's descent to Titan's surface. Nature 438 (8). http://dx.doi.org/10.1038/nature04126.
Turtle, E.P. et al., 2011. Rapid and extensive surface changes near Titan's equator: Evidence of April showers. Science 331, 1414–1417.
Twidale, C.R., 1983. Australian laterites and silcretes: Ages and significance: Revue. Géogr. Phys. Géol. Dynam. 24, 35–45.
Twidale, C.R., 2004. River patterns and their meaning. Earth Sci. Rev. 67, 159–218.
Vail, J.R., 1968. The southern extension of the East African Rift System and related igneous activity. Geol. Rundsch. 57 (2), 601–614.

Wall, S.D. et al., 2009. Cassini RADAR images at Hotei Arcus and western Xanadu, Titan: Evidence for geologically recent cryovolcanic activity. Geophys. Res. Lett. 36, L04203. http://dx.doi.org/10.1029/2008GL036415.

Wall, S. et al., 2010. Active shoreline of Ontario Lacus, Titan: a morphologic study of the lake and its surroundings. Geophys. Res. Lett. 37 (5). http://dx.doi.org/10.1029/2009GL041821. Article ID L05202.

Wellington, J.H., 1955. Southern Africa—A Geographic Study. Physical Geography, vol. 1. Cambridge University Press, U.K., 528p.

Wood, C.A., Lorenz, R., Kirk, R., Lopes, R., Mitchell, K., Stofan, E., Cassini, R.A.D.A.R.Cassini RADAR Team, 2010. Impact craters on Titan. Icarus 206, 334–344. http://dx.doi.org/10.1016/j.icarus.2009.08.021.

Zebker, H.A., Stiles, B., Hensley, S., Lorenz, R., Kirk, R.L., Lunine, J., 2009. Size and shape of Saturn's moon Titan. Science 324, 921–923.

Zernitz, E.R., 1932. Drainage patterns and their significance. J. Geol. 40, 498–521.